Cooperative Dynamics of Motor Proteins on Elastic Cytoskeletal Filaments.

Thesis submitted in partial fulfillment of the requirement for the degree of master of science in the Faculty of Natural Sciences

Submitted by: **Barak Gur**

Advisors: **Prof. Yigal Meir and Dr. Oded Farago**

Department of Physics

Faculty of Natural Sciences

Ben-Gurion University of the Negev

March 13, 2011

Abstract

When many motor proteins work together, they exhibit rather fascinating dynamics. In this work we theoretically study the dynamics of a-polar actin-myosin II systems. Such a-polar systems will show bidirectional dynamics that is composed of directional section. Those directional section have a time length (known as the characteristic reversal time, τ_{rev}) that, before our work, was believed to have an exponential dependent on the size of the system (the number of motors) [1]. However, in a recent experimental work [2], it was found that there is no such exponential dependence. In our work, we suggest that the elasticity of the actin filaments is a key concept that is needed to be taken into account in such systems. We present an *elastic ratchet* model to describe our system and study it both analytically and numerically [3]. By introducing this elasticity, the exponential dependent of the characteristic reversal time is eliminated [3]. Further on, we predict that those elasticity effects will cause a broken symmetry dynamics in certain spatially symmetric configurations of actin-myosin II systems [4]. That is, we show how perfectly a-polar actin-myosin II systems, with specific internal configurations show a bidirectional dynamics with a non vanishing drift velocity.

Contents

Chapter 1

Introduction

1.1 The cell's cytoskeleton and motor proteins

The cytoskeleton is a protein scaffold contained within the cytoplasm. It can be found in most eukaryotic and prokaryotic cells [6, 7]. The eukaryotic cytoskeleton (see Fig. 1.1) consists of three major classes of filaments (see Fig. 1.2): (i) Microtubules which are pipe-like, rigid, hollow, thick structures [8, 9]. The microtubules, like actin filaments, are polar. (ii) Actin filaments which are cable-like, relatively flexible and thin [5]. They are polar and are found mainly in the cortex of the cell. (iii) Intermediate filaments which are rope-like and relatively flexible, the diameter of those filaments is between the diameter of the actin and the microtubule [10–12]. In addition to those three major classes of filaments, the cytoskeleton contains a large collection of accessory proteins that bind to the filaments and either crosslink them together or crosslink the filaments to other cellular structures, such as the plasma membrane, membrane-bound organelles, and chromosomes. The cytoskeleton is a dynamic structure that maintains the cell's structure, this is especially important in animal cells, which have no cell walls and whose fluid-like plasma membrane are unable, on their own, to support complex cellular morphologies.

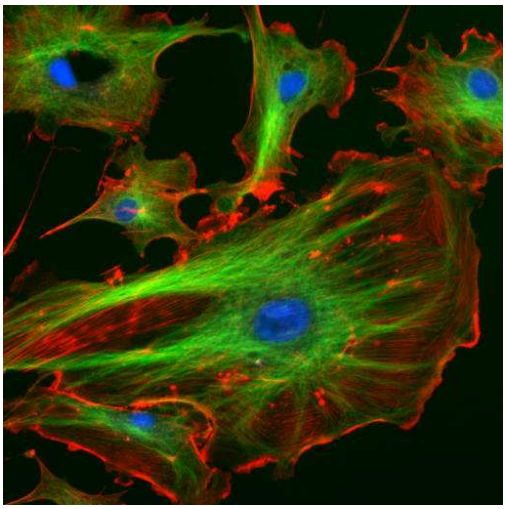

Figure 1.1: The eukaryotic cytoskeleton. Actin filaments are shown in red, microtubules in green, and the nuclei in blue. Figure taken from the U.S Department of Health and Human Services.

In addition to determining the cell's structure, the cell's cytoskeleton serves as tracks for the motor proteins (MPs), which are molecular machines that convert chemical energy derived from ATP hydrolysis into mechanical work. The MPs are the driving force behind most active transports in the cell. They "walk" on the microtubule and actin cytoskeleton and pull vesicles or organelles across the cell [13].

The structure of myosin II is similar for many different types of MPs and consists three major parts:

1. Motor domain (head) - This part is responsible for the interaction with the track and the ATP hydrolysis [14].

2. Neck - This part acts as a lever that amplifies the motion of the head [15].

3. Tail - This acts as a binding site for the cargo.

The rotating crossbridge model, first motivated by the discovery of myosin crossbridges

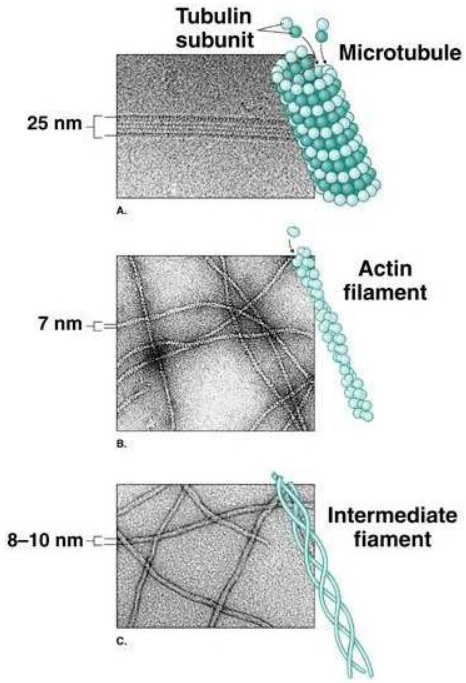

Figure 1.2: The eukaryotic cytoskeleton filaments. (A) The microtubules are pipe-like, rigid, hollow, thick and polar. (B) The actin filaments are cable-like, relatively flexible, thin and polar. (C) The intermediate filaments are rope-like and flexible, and have an intermediate thickness. Image taken from Science Prof Online

in 1957 [16], continues to provide the framework within which the structural, biochemical, and mechanical properties of MPs, not just myosin, can be understood. This model provides a general mechanism for the contraction of muscles, the beating of cilia and flagella, the movement of organelles, and the segregation of the chromosomes. The rotating crossbridge model consists of four cyclic states illustrated in Fig. 1.3.

MPs can be divided into two groups, the members of the first group perform work alone or in groups of small numbers. Dynein and kinesin type motors which use microtubules as track belong to this group of MPs. An example for the work performed by such motors can be seen in the intracellular transport of cargoes which is achieved mainly by the action of

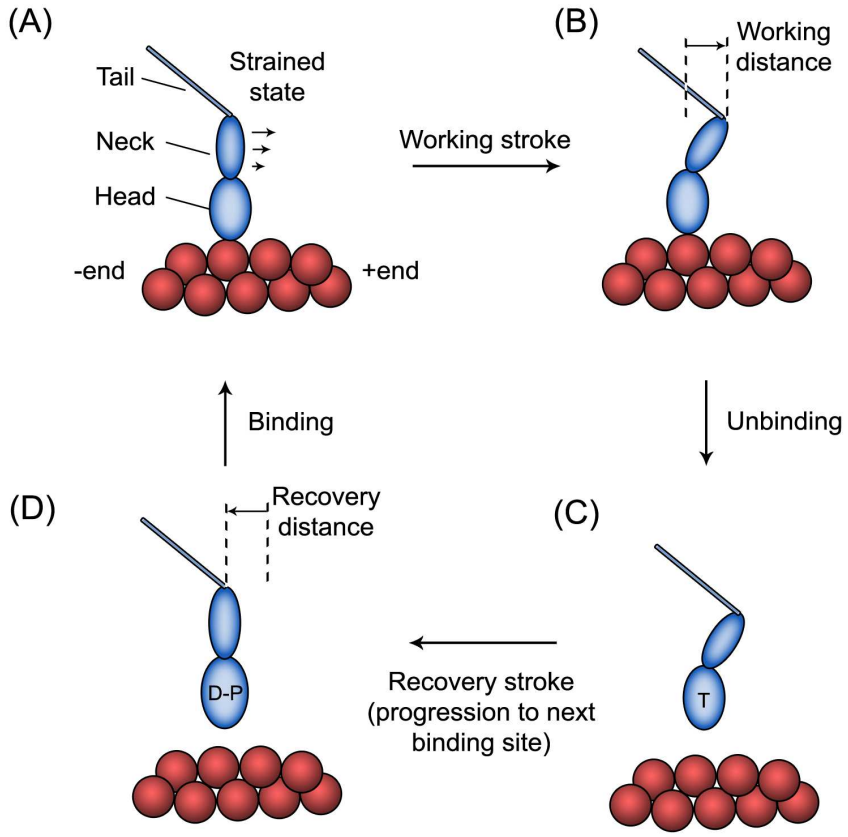

Figure 1.3: The rotating crossbridge model. (A) The binding of myosin to the actin filament catalyzes the release of phosphate from the motor domain and induces the formation of a highly strained ADP state. (B) The strain drives the neck domain, moving the load through the working distance. (C) Following ADP release, ATP binds to the motor domain and causes dissociation of myosin from the actin filament. (D) While dissociated, the crossbridge recovers to its initial conformation, and this recovery moves the motor towards its next binding site on the filament. T=ATP, D=ADP, P=Pi. Figure made by *OP designs*.

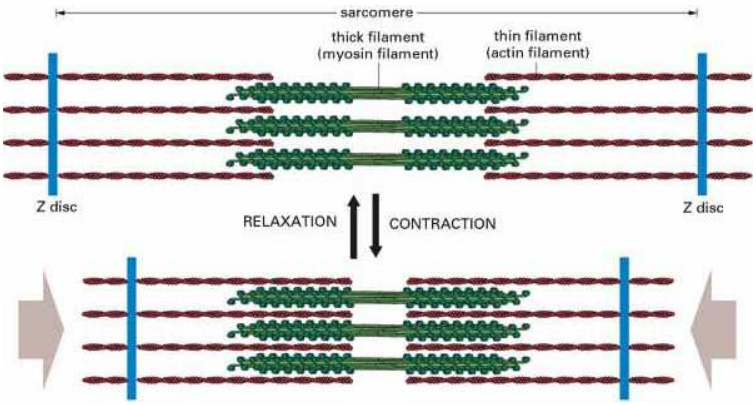

Figure 1.4: The sarcomere is composed from thick myosin bundles and thin actin filaments. The two states are shown, the relaxed state, the upper part of the picture, and the contracted state, the lower part of the picture, which is caused as a result of the relative movement between the myosin bundles and the actin filaments. Image taken from Bora Zivkovic's lecture notes.

individual motors that propagate along the cytoskeleton tracks in a direction determined by the intrinsic polarity of the filaments [38]. To the other group of MPs-the group on which we will focus in our work-belong myosin type motors which use actin filaments as tracks. The members of this group perform work in groups of large numbers and show characteristics of a complex system[1]. Examples for the cooperative work of MPs that belong to the second group can be seen in the anatomical unit of a muscle, the sarcomere (see Fig. 1.4), that contains thousands of myosin motors forming a thick filament and acting together, pulling on attached actin filaments and causing them to slide against each other [39]. Furthermore, MPs of the second kind form and close the contraction ring in the mitosis process, see Figs. 1.5, 1.6.

[1]The term complex system in this context refers to a system that as a whole, exhibit one or more properties not obvious from the properties of its individual parts.

1.2 In vitro motility assay

An in vitro motility assay is a technique in which the motility of purified MPs along purified cytoskeletal filaments is reconstituted in cell-free conditions. Then, the dynamics is studied, usually by the assistant of fluorescence. An important development of this technique, and an almost in vitro motility assay, was done in 1983 by Shetz and Spudich [40], were the dynamics of beads coated with purified myosin upon actin cables in the cytoplasm of the alga *Nitella* was visualized using fluorescence. The following big development has been published in 1985 by Spudich et al. [41], where the first completely reconstituted assay in which motor-coated beads were shown to move along the actin filaments made from purified actin that had been bound to the surface of a microscope slide.

The two geometries used when doing in vitro motility assays are the bead assay and the gliding assay. In the bead assay, filaments are fixed to a substrate, such as a microscope slide, and motors are attached to small plastic or glass beads. Then, in the presence of ATP, the motion of the beads is visualized by a light microscope. In the gliding assay, the motors are the ones which are fixed to the substrate and the filaments are placed on top of them and their motion is observed. The fluorescence technique has been developed to a level were it is even possible to image individual fluorescently labeled motors [44] and watch them move along the filaments [45, 46].

1.3 Ratchet models for motor dynamics

1.3.1 The perpetuum mobile

When discussing ratchet models, it is worth to mention the perpetuum mobile of the second kind. This machine can, supposedly, extract work out of a thermal bath violating the

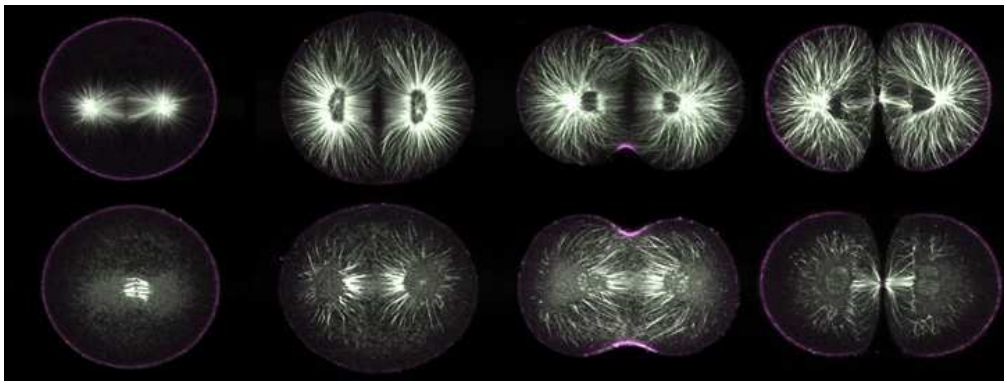

Figure 1.5: Purple urchin zygotes during first mitosis, fixed and stained for microtubules (white) and phosphorylated myosin II (magenta; single confocal sections). Top row: metaphase, anaphase, telophase, and furrowing completed, in untreated cells. Bottom row: zygotes of equivalent stages, but treated five minutes before fixation with nocodazole. In metaphase, only kinetochore fibers survive nocodazole treatment; the astral microtubules all disappear. In anaphase, however, some astral microtubules remain, and during telophase it is apparent that most of these point toward the equator (third panel, bottom row). Figure taken from the center for cell dynamics, university of Washington

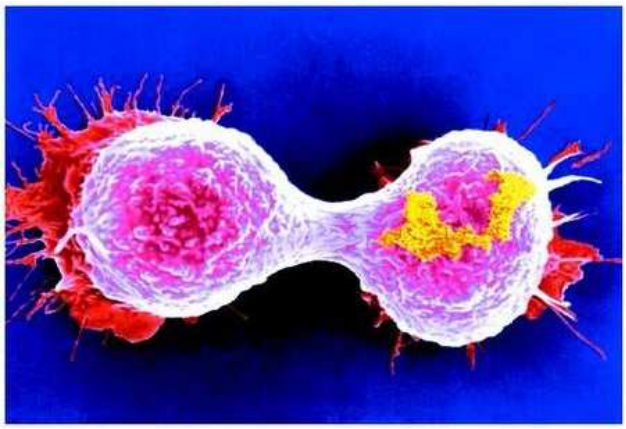

Figure 1.6: A colored scanning electron micrograph of a breast cancer cell mitosis. Figure taken from Biology Reference.

second law of thermodynamics[2]. This idea of extracting work out of a thermal bath was first addressed in a conference talk given by Smoluchowski in Münster 1912 (published as proceedings-article [42]) and was later popularized and extended in Feynmans Lectures on Physics [43]. In order to convert Brownian motion into useful work, they have suggested the following *Gedankenexperiment* (A thought experiment) illustrated in Fig. 1.7. An axle is connected to paddles at one end and a ratchet at the other end. The ratchet is restricted by a pawl to rotating in only one direction (see Fig. 1.7), and the whole device is surrounded by a gas at thermal equilibrium. It seems rather convincing, that when the gas particles hit the paddles, the device will rotate in only one direction (because of the pawl) and therefore, it would allow to extract work out of the thermal bath. However this expectation is wrong: In spite of the built in asymmetry, no preferential direction of motion is possible. Otherwise, this would be in marked contradiction to the second law of thermodynamics. As Smoluchowski points out [42], since the impacts of the gas molecules take place on a microscopic scale, the pawl needs to be extremely small and soft in order to admit a rotation even in the forward direction. Because of this, the pawl itself is therefore also subjected to non-negligible random thermal fluctuations. So, every once in a while the pawl lifts itself up and the saw-teeth can freely travel underneath allowing it to rotate backwards and "unwind" the lift back down.

An experimental Realization of this *Gedankenexperiment* has been done on a molecular scale by Kelly et al. [47–49]. Their synthesis of triptycene (4)helicene incorporates into a single molecule all essential components: The triptycene paddlewheel functions simultaneously as circular ratchet and as paddles, the helicene serves as pawl and provides the necessary asymmetry of the system. Both components are connected by a single chemical bond, giving rise to one degree of internal rotational freedom. By the use of nuclear magnetic resonance (NMR), the predicted absence of a preferential direction of rotation at thermal equilibrium

[2]Perpetuum mobile of the first kind is a machine that violates the first law of thermodynamics, conservation of energy.

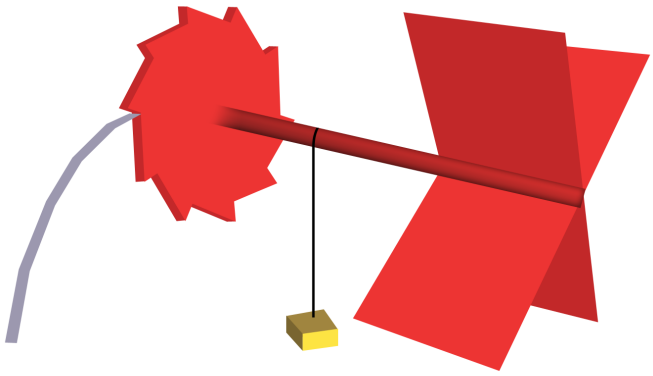

Figure 1.7: Ratchet and pawl. The ratchet is connected by an axle with the paddles and with a spool, which may lift a load. In the absence of the pawl (leftmost object) and the load, the random collisions of the surrounding gas molecules (not shown) with the paddles cause an unbiased rotatory Brownian motion. The pawl is supposed to rectify this motion so as to lift the load. Figure made by *OP designs*.

has been experimentally confirmed.

1.3.2 Ratchet model for a single motor

According to the second law of thermodynamics, heat cannot be converted into work in an isothermal system, this has been illustrated by Feynman [43] via the *Gedankenexperiment* that has been discussed in subsection 1.3.1. One of the outcomes of the second law of thermodynamics is that a particle which is placed in a thermal bath will diffuse randomly, showing a Brownian motion with a vanishing mean displacement and speed. Even if an asymmetric, but homogeneous on a macroscopic scale, potential is applied in the system, a directed motion will not be induced as illustrated in Fig. 1.8. Therefore, in order to generate a directed motion at a constant temperature, it is necessary to have an energy source and drive the system out of equilibrium. Over the years, different ratchet models have been

used in order to generate such a directed motion. These works are divided into three types, according to the origin of the energy source:

(i) *Fluctuating forces:* a point-like particle is places in a periodic, asymmetric potential $U(x)$ and is submitted to a fluctuating, zero average force, $< F(t) >= 0$, but with a richer correlation function than a simple Gaussian white noise. These correlations of the fluctuating forces reflect the energy source. Typically the particle motion is described by Langevin equation:

$$\lambda \frac{dx}{dt} = \partial_x U(x) + F(t), \tag{1.1}$$

were x is the position of the particle and λ is the friction coefficient. Once the fluctuation dissipation theorem is broken, a rectified motion sets in [17–28].

(ii) *Fluctuating potential:* a point-like particle is placed in a periodic, asymmetric potential with a value that depends on time:

$$\lambda \frac{dx}{dt} = \partial_x U(x,t) + f(t). \tag{1.2}$$

x, λ, and U have the same meaning as in Eq. 1.1 but the potential depends explicitly on time, and the random forces $f(t)$ are Gaussian white noise which obeys a fluctuation-dissipation theorem: $< f(t) >= 0$, and $< f(t)f(t') >= 2\lambda T\delta(t-t')$. In these works, the potential's explicit dependence on time reflects the energy source. Most works have considered the case in which $U(x,t) = A(t)V(x)$ [29–32]

(iii) *Particle fluctuating between states:* the point-like particle transits between well-defined states [33–37]. In each of the states, the particle experiences a classical Langevin equation:

$$\lambda_i \frac{dx}{dt} = \partial_x U_i(x) + f_i(t). \tag{1.3}$$

The index i refers to the considered state, and $f_i(t)$ satisfies a fluctuation-dissipation theorem: $< f_i(t) >= 0$, and $< f_i(t)f_j(t') >= 2\lambda T\delta(t-t')\delta_{ij}$. The dynamics of transitions between the

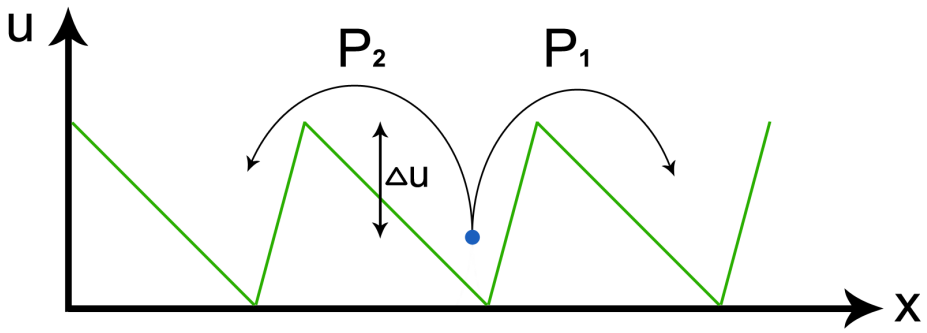

Figure 1.8: A particle (in blue) is placed in an asymmetric potential. However, there is no energy source in this system. The particle will spend most of the time near one of the minima. Occasionally, it will hop from one well to its neighbor. The probability of the particle hopping to the right/left neighbor depends only on the energy gap, Δu, and does not depend on the slope of the potential. Therefore $P_1(\Delta u) = P_2(\Delta u)$ and the particle will show a vanishing mean displacement and speed. Figure made by *OP designs*.

states is added independently, and reflects the energy source.

We conclude that all the three types of models presented above have an asymmetric potential which models the polarity of the track on which the motor walks. In addition, all of those models have some kind of an energy source which drives the system out of equilibrium. The combination of these two is sufficient in order to generate a biased dynamics.

1.3.3 Ratchet model for collective motor dynamics

Ratchet models can be generalized to describe the collective dynamics of motors. For those models, the particles can be taken to either have motor-motor interactions [50–53] or have no such interactions. For the noninteracting case, the coupling is achieved by attaching the particles, in a rigid or flexible connection, to a "backbone" while keeping the two-state

model for each one of them [54]. The collective dynamics of motors is influenced by both the motor-motor interactions [55] and the mechanical coupling, as illustrated in the model proposed by Badoual at al. [1] (and which, we will present a slightly modified version of). Ratchet models are also used to describe cooperative bidirectional dynamics. This dynamics is characterized by a vanishing bias (this can be achieved by taking a symmetric potential) but consists of long directional sections, where only on large time scales the dynamics can be seen as bidirectional. The characteristic time it takes for the motion to change its direction is marked as τ_{rev}. Of special interest is the theoretical work of Badoual at al. [1] where τ_{rev} is found to have an exponential dependence on N, the number of motors. This means that, for a symmetric potential, τ_{rev} will diverge in the thermodynamic limit, $N \to \infty$. That is, the system will exhibit a unidirectional motion in the direction that has been spontaneously chosen at $t = 0$.

1.4 Outline

The thesis is organized as follows: In chapter 2 we study the bidirectional cooperative dynamics. We will introduce a *thermal ratchet* for the cooperative dynamics of MPs. The model will be treated by means of computer simulations and analytical treatment. Our model will reconstruct the divergence of the reversal time, τ_{rev}, in the thermodynamic limit. This result is in marked contradiction to recent experimental results regarding the cooperative dynamics of a-polar actin-myosin systems. Those experiments show no such strong dependence of the reversal time, τ_{rev}, on N, the number of motors [2]. We will suggest to solve this contradiction by modifying our model so it will take into account the elastic energy of the actin filaments [3]. This will have a strong influence on the cooperative dynamics and eliminate the exponential dependence of the reversal time, τ_{rev}, on N, the number of motors. Further on, in chapter 3, we will introduce a theoretical prediction, showing how this elasticity will introduce an additional cooperative effect that will cause a symmetry braking

in the dynamics of certain spatially symmetric systems, that is, we will show that certain perfect a-polar actin-myosin systems will exhibit a biased asymmetric dynamics due to this elastic cooperative effect.

Chapter 2

Bidirectional motion of a-polar filaments

One of the more interesting outcomes of cooperative action of MPs is their ability to induce bidirectional motion. "Back and forth" dynamic has been observed in various motility assays including: (i) myosin II motors walking on actin tracks with randomly alternating polarities [2], (ii) NK11 (kinesin related Ncd mutants which individually exhibit random motion with no preferred directionality) moving on microtubules (MTs) [56], (iii) mixed population of plus-end (kinesin-5 KLP61F) and minus-end (Ncd) driven motors acting on MTs [57], and (iv) myosin II motors walking on actin filaments in the presence of external stalling forces [58]. Reversible transport of organelles through the combined action of kinesin II, dynein, and myosin V has been also observed in *Xenopus* melanophores [59]. In the latter example, the kinesin and dynein move the organelle in opposite directions along MTs, while the myosin motors (which take the organelle on occasional "detours" along the actin filaments) function as "molecular ratchets", controlling the directionality of the movement along the MT transport system. From a theoretical point of view, cooperative dynamics of molecular motors and, in particular, bidirectional movement, have been investigated using several

distinct models including ratchet models that have been discussed in section 1.3. Other theoretical approaches are the lattice and continuum asymmetric exclusion models [50, 60–65], and the tug-of-war model which has been recently proposed for describing the transport of cargo by the action of a few motors [66–69]. The common theme in these experimental and theoretical studies is the association of bidirectionality with the competition between two populations of motors that work against each other to drive the system in opposite directions. The occasional reversals of the transport direction reflect the "victory" of one group over the other during the respective time intervals. The balance of power is shifting between the two motor parties as a result of stochastic events of binding and unbinding of motors to the cytoskeletal track. Without going into the details of the various existing models of cooperative bidirectional motion, we note that most of them assume that the motors interact mechanically but act independently, i.e., their binding to and unbinding from the track are uncorrelated. By further assuming that the attachment and detachment events of individual motors are Markovian, the distribution of "reversal times" (i.e., the durations of unidirectional intervals of motion) can be shown to take an exponential form

$$p(\delta t) = \exp(-\delta t/\tau_{\rm rev}), \tag{2.1}$$

were $\tau_{\rm rev}$ is the characteristic reversal time of the bidirectional motion.

2.1 Bidirectional cooperative motion of myosin-II motors on a-polar actin tracks

2.1.1 Experimental setup

This exponential distribution of "reversal times" (Eq. 2.1) has recently been measured in a novel motility assay [2]. The setup of this motility assay contains two stages, in the

first stage, the surface of a microscope slide was saturated by BSA[1] and NEM myosin II. Then, actin filaments/bundles were attached to, and on top of the NEM myosin motors as illustrated in Fig. 2.1. In the second stage, myosin II minifilaments (multi-headed brown objects, Fig. 2.2A) were added to the cell sample. This caused the severing of small polar actin fragments that fused together with other short actin fragments of the opposite polarity, creating new, longer, a-polar, bundles as described in details in Fig 2.2. The rate of fusion events decreased with time and, after several minutes, the system relaxed into its final configuration, shown schematically in Fig. 2.2F. Notice that the severing and rearrangement of the originally formed actin filaments/bundles (Fig. 2.1B) led to the formation of much shorter bundles (Figs. 2.2B-E). Moreover, the random nature of the multiple fusion processes involved in the generation of these shorter bundles ensured that the final actin tracks were highly a-polar.

2.1.2 Experimental results

The motion of the a-polar actin filaments was visualized by fluorescence microscopy. Fig. 2.3A shows the position of center of mass of one bundle (three snapshots are shown in Figs. 2.3B-D) during a period of more than 10 minutes of the experiment. The dynamics of this bundle are representative of the motion of the other actin bundles. Measurements of the position of the center of mass of the bundle were taken at time intervals of $\Delta t = 2$ sec, and the mean velocity in each such period of motion was evaluated by $v = \Delta x/\Delta t$, where Δx is the displacement of the center of mass. Fig. 2.4A shows the velocity histogram of the bundle shown in Fig. 2.3. The velocity histogram is bimodal indicating that the motion is bidirectional. The speed of the bundle varies between $|v| = 1 - 2$ μm/min, which is 2 orders of magnitude lower than the velocities measured in gliding assays of polar actin filaments on myosin II

[1] the BSA is used to immobilize the Nem myosin II motors.

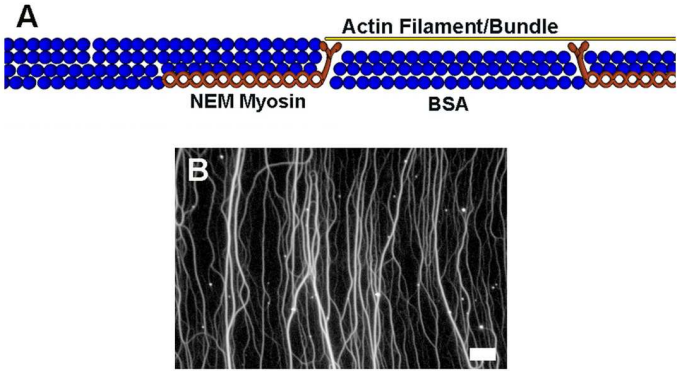

Figure 2.1: (A) Schematic diagram of the system before addition of active motors. The blue balls mark the BSA and the thin yellow line is the actin filament/bundle. The actin filaments are attached to brown, long, two-headed objects which are the NEM myosin. (B) An image of the system before the addition of active myosin II. The long curved vertical objects are the actin filaments. Bar size is 5 μm. Figure taken from Gilboa et al. [2].

motors[2] [70]. The bidirectional movement consists of segments of directional motion which typically last between 2 to 10 time intervals of $\Delta t = 2$. The statistics of direction changes is summarized in Fig. 2.4B which shows a histogram of the number of events of directional movement of duration t. The characteristic reversal time, $\tau_{\rm rev}$, can be extracted from the histogram by a fit to an exponential distribution, Eq.2.1.

[2]The fact that the typical speed of the bidirectional motion is considerably smaller than those of directionally-moving polar actin filaments can be partially attributed to the action of individual motors working against each other in opposite directions.

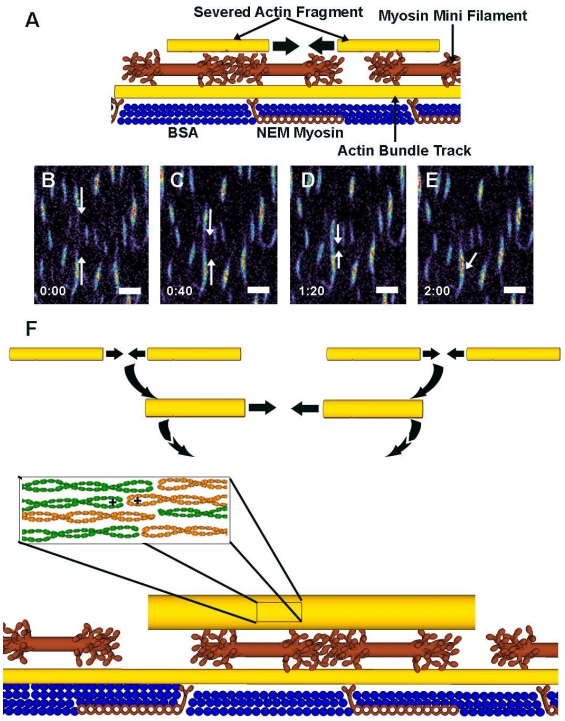

Figure 2.2: (A) Schematic diagram of the system after addition of active myosin II motors. After the first stage (see Fig. 2.1), myosin II minifilaments (multi-headed brown objects) were added to the sample. The motors that landed on the BSA surface created a homogeneous bed of immobile, yet active, motors. Other motors landed on the actin filaments (long yellow line), and started to move along it. During their motion, the motors exerted forces on the actin filaments, which caused severing of small actin fragments (short yellow lines). The ruptured actin fragments could move rapidly on the bed of active myosin II minifilaments and fuse with other bundles. One fusion event is demonstrated in the sequence of snapshots (B-E). Here, are shown (B) two bundles moving oppositely to each other, getting closer (C) and then fusing (D-E) to create one larger object. Time is given in minutes, bar size is 5 μm. (F) The bundles continue to grow in size through multiple fusion processes, until eventually a large, highly a-polar bundle is formed (thick yellow tube - the inset illustrates the internal structure of such a bundle, consisting of individual actin filaments with randomly orientated polarities). Figure taken from Gilboa et al. [2].

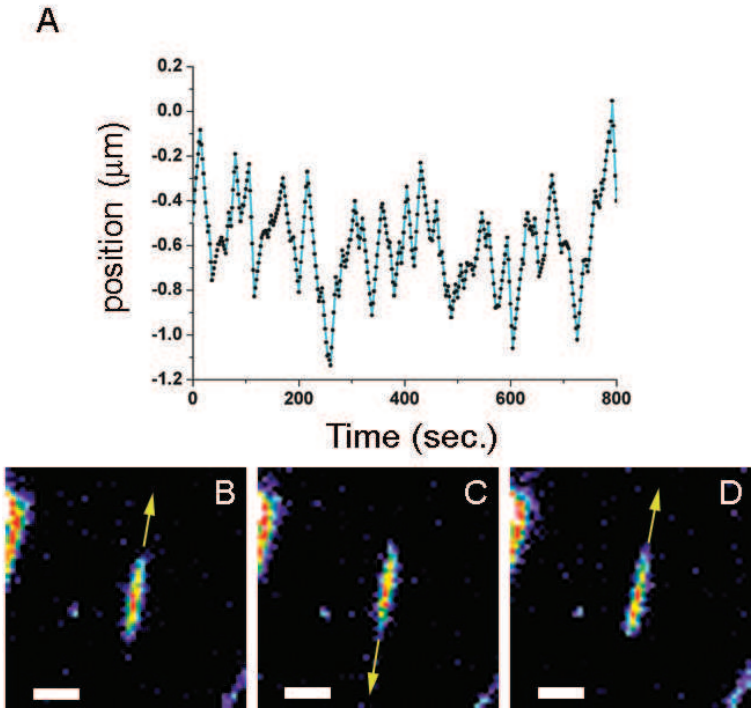

Figure 2.3: Position of a bundle over a time interval of 800 sec. The time interval between the consecutive data points is 2 sec. (B-D) Pseudo-color images of the actin bundle. The yellow arrows indicate the instantaneous direction of motion of the bundle. Bar size is 5 μm. Figure taken from Gilboa et al. [2].

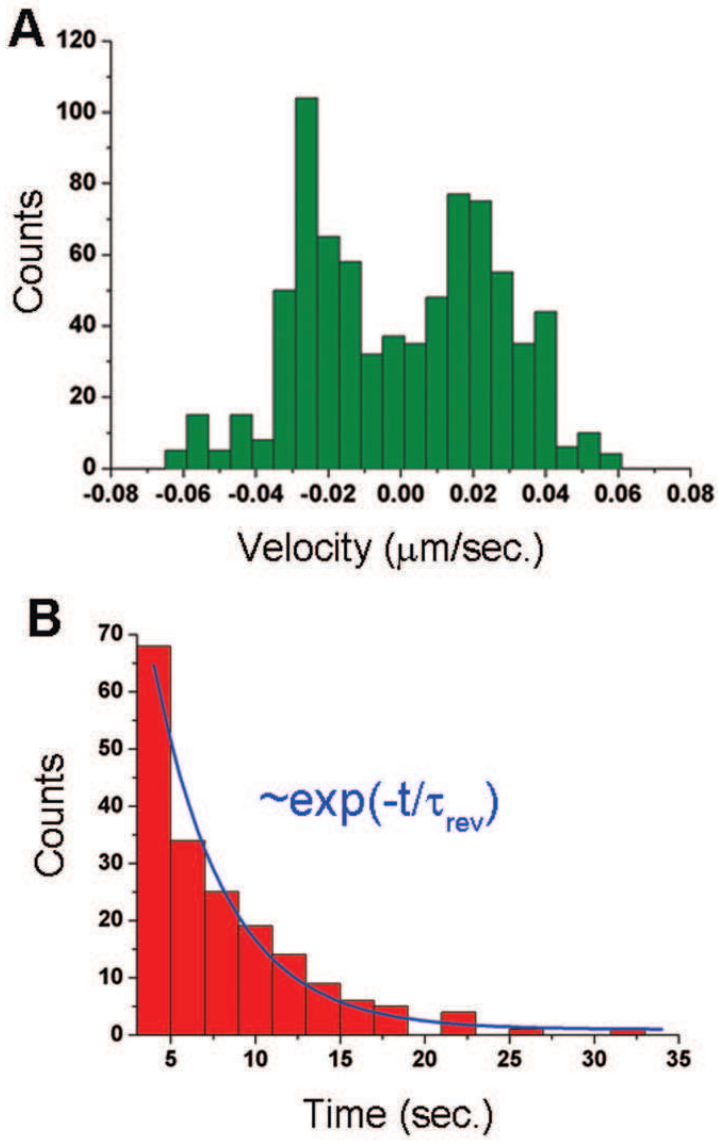

Figure 2.4: Velocity histogram of the bundle whose motion is shown in Fig. 2.3 (based on 900 sampled data points - Fig. 2.3 shows only 400 of those points), exhibiting a clear bimodal distribution. (B) Distribution of the reversal time for the same bundle. The distribution is fitted by a single exponential decay function with a characteristic reversal time: $\tau_{\text{rev}} \sim 3$ sec. Figure taken from Gilboa et al. [2].

2.2 A ratchet model for the cooperative dynamics of molecular motors

Our model is a modified version of the original model of Badual et al. [1] which was presented in section 1.3. Our model is illustrated schematically in Fig. 2.5: We consider the 1D motion of a group of N point particles (representing the motors) connected to a rigid rod with equal spacing q. The actin track is represented by a periodic saw-tooth potential, $U(x)$, with period l and height H. We choose $q = (5\pi/12)l \sim 1.309l$, this choice is motivated by the incommensurate arrangement of motors and filaments in muscle fibers [1, 54]. The locally preferred directionality of the myosin II motors along the actin track is introduced via an additional force of size f_{ran} exerted on the individual motors when attached to the track. In each unit of the periodic potential, this force randomly points to the right or to the left (the total sum of these forces vanishes), which mimics the random, overall a-polar, nature of the actin bundles in our experiments.

The instantaneous force between the track and the motors is given by the sum of all the forces acting on the individual motors:

$$F_{\mathrm{tot}} = \sum_{i=1}^{N} f_i^{\mathrm{motor}} = \sum_{i=1}^{N} \left[-\frac{\partial U\left(x_1 + (i-1)\, q\right)}{\partial x} + f_{\mathrm{ran}}\left(x_1 + (i-1)\, q\right) \right] \cdot C_i(t), \tag{2.2}$$

where $x_i = x_1 + (i-1)q$ is the coordinate of the i-th motor. The two terms in the square brackets represent the forces due to the symmetric saw-tooth potential and the additional random local forces acting in each periodic unit. The latter are denoted by red arrows in Fig. 2.5A. The function $C_i(t)$ takes two possible values, 0 or 1, depending on whether the motor i is detached or attached to the track, respectively, at time t. The group velocity of the motors (relative to the track) is determined by the equation of motion for overdamped dynamics:

$$v(t) = F_{\mathrm{tot}}(t)/\lambda, \tag{2.3}$$

Were the friction coefficient, λ, depends mainly on motors attached to the track at a certain moment and is therefore proportional to the number of connected motors, $N_c \leq N$ at time t: $\lambda = \lambda_0 N_c$.

To complete the dynamic equations of the model, we need to specify the transition rates between states (0 - detached; 1 - attached). The motors change their states independently of each other. We define an interval of size $2a < l$ centered around the potential minima (the gray shaded area in Fig. 2.5). If in one of these regions, an attached motor may become detached ($1 \rightarrow 0$) with a probability per unit time ω_1. Conversely, a detached motor may attach to the track ($0 \rightarrow 1$) with transition rate ω_2 only if located outside this region of size $2a$. However, we also allow another independent route for the detachments of motors, which may take place outside the gray shaded area in Fig.2.5 (i.e., around the potential maxima) and is characterized by an off rate ω_3. The rates ω_1, ω_2, ω_3 (see blue arrows in Fig.2.5), represent the probabilities per unit time of a motor to (i) detach after completing a unit step, (ii) attach to the track, or (iii) detach from the track without completing the step.

2.2.1 Filament's elasticity

One of the most important characteristics that our model shares with the original model of Badual et al. [1] is that the attachment and detachment rates are constants. Because of this, the reversal time, τ_{rev}, depends exponentially on the number of motors, N. However, the experimental results of Gilboa et al. [2], presented in Fig. 2.6, clearly contradict this theoretical prediction, and therefore, we conclude that our model is missing something. Generally speaking, the rates of transitions between states depend on many biochemical parameters, most notably the types of motors and tracks, and the concentration of chemical fuel (e.g., ATP). They may also be affected by the forces induced between the motors and the filament, which result in increase in the configurational energy of the attached myosin motors [71–74] and in the elastic energy stored in the S2 domains of the mini-filaments, as well

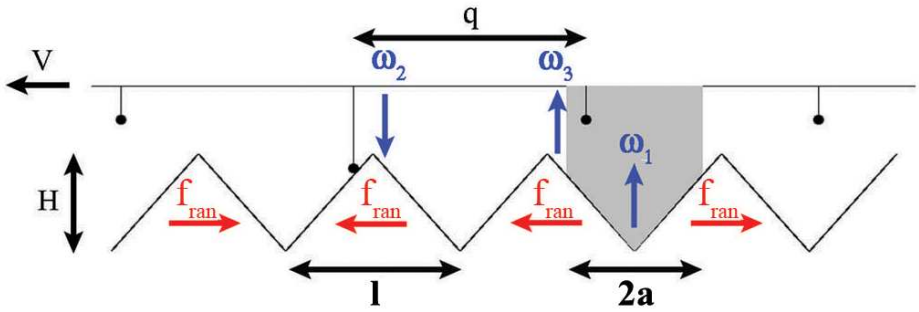

Figure 2.5: N point particles (representing the motors) are connected to a rigid rod with equal spacing q. The motors interact with the actin track via a periodic, symmetric, saw-tooth potential with period l and height H. In each periodic unit, there is a random force of size f_{ran}, pointing either to the right or to the left. The motors are subject to these forces only if connected to the track. The detachment rate ω_1 is localized in the shaded area of length $2a < l$, while the attachment rate ω_2 is located outside of this region. The off rate ω_3 is also located outside the gray shaded area.

as an increase in the stretching energy of the actin filament. The latter contribution can be introduced into the model via a modified detachment rate given by: $\omega_3 = \omega_3^0 \exp(-\Delta E/k_B T)$, where ΔE is the change in the elastic energy of the actin track due to the detachment of one motor head. The dependence of ΔE on the number of connected motors N_c (out of a total number of motors, N) can be estimated in the following manner: Consider a series of $N+1$ point particles connected by N identical springs (representing a series of sections of actin filaments) having a spring constant k (see Fig. 2.7). Let us assume that random forces act on the particles and denote the force applied on the particle with index l ($1 \leq l \leq N+1$) by f_l. Assume that each of these forces can take three possible values: $-f$ (representing attached motors locally pulling the track to the left), $+f$ (attached motors pulling the track to the right), and 0 (detached motors not applying force). Defining the "excess force" with respect to the mean force acting on the particles: $f_l^* = f_l - \bar{f}$ (where $\bar{f} = \sum_{i=1}^{N+1} f_l/(N+1)$), one can show that the force stretching (or compressing) the i-th spring in the chain is given by the sum of excess forces acting on all the particles located on one side of the spring

$$F_i = \sum_{l=1}^{i} f_l^* = -\sum_{l=i+1}^{N+1} f_l^*. \tag{2.4}$$

From Eq. 2.4 it can be easily verified that $\sum_{i=1}^{N} F_i = 0$. We thus conclude that the excess forces acting on the particles, f_l^*, represent a series of random quantities with zero mean. Therefore, the size of F_i can be estimated by mapping the chain of springs into the problem of a 1D random polymer ring [75], where the elastic energy stored in the i-th spring, $\epsilon_i = F_i^2/2k$, plays the role of the squared end-to-end distance between the $i+1$ monomer and the origin. From this mapping we readily conclude that the energy of most of the springs (except for those located close to the ends of the chain) scales linearly with the number of attached motors: $\epsilon \sim N_c(f^2/2k)$. The total elastic energy of the chain scales as

$$E \sim N\epsilon \sim NN_c(f^2/2k), \tag{2.5}$$

and when a motor detaches from the track ($N_c \to N_c - 1$),

$$\Delta E/k_BT = -\alpha N \tag{2.6}$$

where α is a dimensionless prefactor.

2.2.2 Model parameters

We simulated the dynamics of an N-motor system, choosing parameters corresponding to the myosin II-actin system. The period of the potential $l = 5$ nm corresponds to the distance between binding sites along the actin track [76–78], and therefore $q = 6.54$ nm (see section 2.2). The force generated by each motor head on the track is $2H/l = 5$ pN (first term in square brackets in Eq. 2.2). The magnitude of the random force that defines the local polarity of the track (second term) is given by $f_{\text{ran}} = 1$ pN, so the total force acting on each motor head ranges between about 4 to 6 pN [76, 77, 79, 80]. The interval around the potential minima from which motors can detach from the track with rate ω_1 is chosen to be $2a = 3.8$ nm. The transitions rates between attached and detached states are $\omega_1^{-1} = 0.5$ ms and $\omega_2^{-1} = 33$ ms [39, 81–83]. With this choice of parameters, we obtain a system with a low fraction of attached motors (see later Fig. 2.12) which is characteristic for nonprocessive myosin II motors. We also set the friction coefficient per attached motor to $\lambda_0 = 85 \cdot 10^3$ kg/s, which yields the velocity $v \sim 0.02$ μm/s (see later the insets of Fig 2.8A). The rate ω_3^0 expresses the probability of a single motor head to detach from the track without advancing to the next unit. The probability $\tilde{p}$ of such an event is 1-2 orders of magnitude smaller than the complementary probability $(1 - \tilde{p})$ to execute the step. We take $\tilde{p} = 1/30$ [83], which yields$(\omega_3^0)^{-1} \sim (pv/l)^{-1} = 7500$ ms. Finally, the exponent α appearing in Eq. 2.6 is evaluated by:

$$\alpha \sim (f^2/2kk_BT) = (f^2 l/2YAk_BT), \tag{2.7}$$

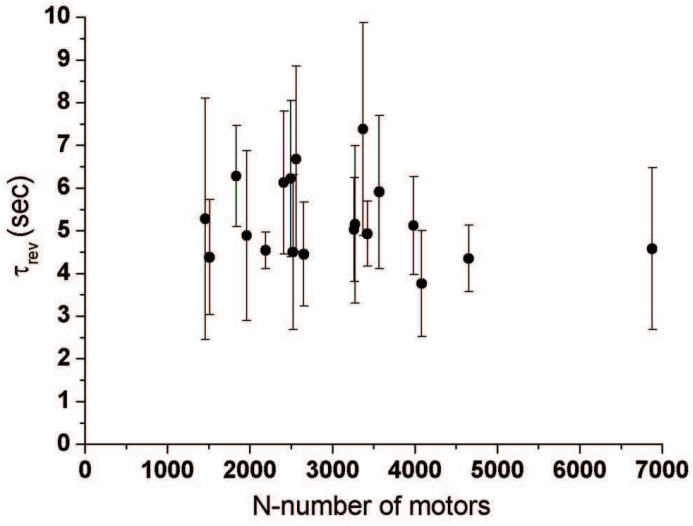

Figure 2.6: Characteristic reversal time, $\tau_{\rm rev}$, of 19 different bundles as a function of the number of working motors N. The reversal time for each bundle is obtained by an exponential fit as shown in Fig.2.4B. Figure taken from Gilboa et al. [2].

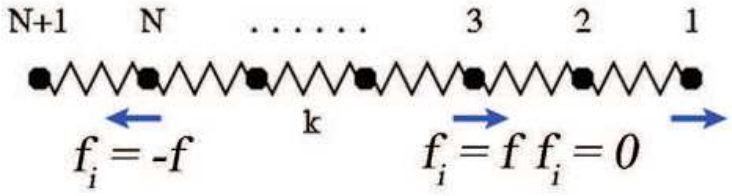

Figure 2.7: A schematic drawing of the system: A chain of consisting of $N+1$ monomers connected by with alternating polarities. The monomers are connected to each other by N identical springs. The chain lies on a "bed" of motors, some of which are connected to the monomers. A connected monomer with positive (negative) polarity feels a pulling force of size $+f$ $(-f)$. Disconnected monomers experience no force. Figure taken from Gilboa et al. [2].

where $Y \sim 10^9$ Pa is Young's modulus for actin and $A \sim 35$ nm^2 is the cross sectional area of an actin filament [83]. For the model parameters $\alpha \sim 0.002$. There is some freedom in choosing the model parameters, fortunately, our model does not show a strong dependence on most of those parameters. One exception is the value of α which is somewhere between 0.0015 and 0.0025, we have chosen to work with the intermediate value, $\alpha \sim 0.002$. Later in this work, in the end of section 2.4, we will show the dependence of our results for solving the model using slightly different model parameters.

2.3 Computer simulations

The model presented in section 2.2 has been investigated by means of Metropolis Monte Carlo simulations by Gillo et al. [3]. In order to simulate conditions corresponding to the dynamics of a-polar tracks, they randomly chose the direction of the random force (the force representing the local polarity of the track, see horizontal red arrows in Fig. 2.5) in each unit cell, but discarded the tracks at which the sum of random forces did not exactly vanish. They computationally measured the characteristic reversal time, τ_{rev}, as a function of N in the range of $400 \leq N \leq 2400$. For each value of N, they generated 40 different realizations of random tracks and simulated the associated dynamics for a total period of $2 \cdot 10^5$ seconds. During this period of time they followed the changes in the direction of motion and calculated the probability distribution function (PDF) of the reversal times. The characteristic reversal time corresponding to each random track was extracted by fitting the PDF to an exponential form (see Eq. 2.1), as demonstrated in Fig. 2.8A. Fig. 2.8B summarizes the results, where here, for each N, the reversal time plotted (denoted by $\langle \tau_{\text{rev}} \rangle$) is the average of τ_{rev} calculated for the different track realizations. The error bars represent the standard deviation of τ_{rev} between realizations. The data points depicted in solid circles correspond to $\alpha = 0.002$, while the open circles correspond to $\alpha = 0$, i.e., to the model originally presented in ref. [1]

where the on and off rates defined in Eqs. 2.9 and 2.10 do not dependent on N. The mean reversal time $\langle \tau_{\rm rev} \rangle$ exhibits a very strong exponential dependence on N for the case of $\alpha = 0$ as shown by the straight line in Fig. 2.8B. Because of this very rapid increase of $\langle \tau_{\rm rev} \rangle$ with N, the reversal times (in the $\alpha = 0$ case) could not be accurately measured for $N > 1800$. Based on the exponential fit (solid line in Fig. 2.8B), the mean reversal time for $N = 2400$ is estimated to be of the order of a few hours. In contrast, the calculated $\langle \tau_{\rm rev} \rangle$ corresponding to $\alpha = 0.002$ show a non-monotonic dependence on N. The computed $\langle \tau_{\rm rev} \rangle$ are much smaller in this case, and fall below 1 minute for all values of N.

2.4 Analytical treatment

In the following section we use a master equations to analyze the bidirectional motion exhibited by the computational simulations. This analytical approach corresponds to the limit $N \gg 1$ where one can introduce the probability densities $p_{\rm att}(x)$ and $p_{\rm det}(x)$ of finding a motor in the attached or detached state, respectively, at position $-l/2 < x \leq l/2$ within the unit cell of the periodic potential. These probability densities are the steady-state solutions of the following set of coupled master equations which govern the transitions between the two connectivity states:

$$\begin{cases} \partial_t p_{\rm att}(x,t) + v\partial_x p_{\rm att}(x,t) = -\omega_{\rm off}(x) p_{\rm att}(x,t) + \omega_{\rm on}(x) p_{\rm det}(x,t) \\ \partial_t p_{\rm det}(x,t) + v\partial_x p_{\rm det}(x,t) = -\omega_{\rm on}(x) p_{\rm det}(x,t) + \omega_{\rm off}(x) p_{\rm att}(x,t). \end{cases} \tag{2.8}$$

Were v is the group velocity of the motors and $\omega_{\rm on}(x)$ and $\omega_{\rm off}(x)$ denote the space-dependent on and off rates defined as

$$\omega_{\rm on}(x) = \begin{cases} 0 & |x| \leq a \\ \omega_2 & a < |x| \leq l/2 \end{cases} \tag{2.9}$$

and

$$\omega_{\rm off}(x) = \begin{cases} \omega_1 & |x| \leq a \\ \omega_3^0 \exp(\alpha N) & a < |x| \leq l/2. \end{cases} \tag{2.10}$$

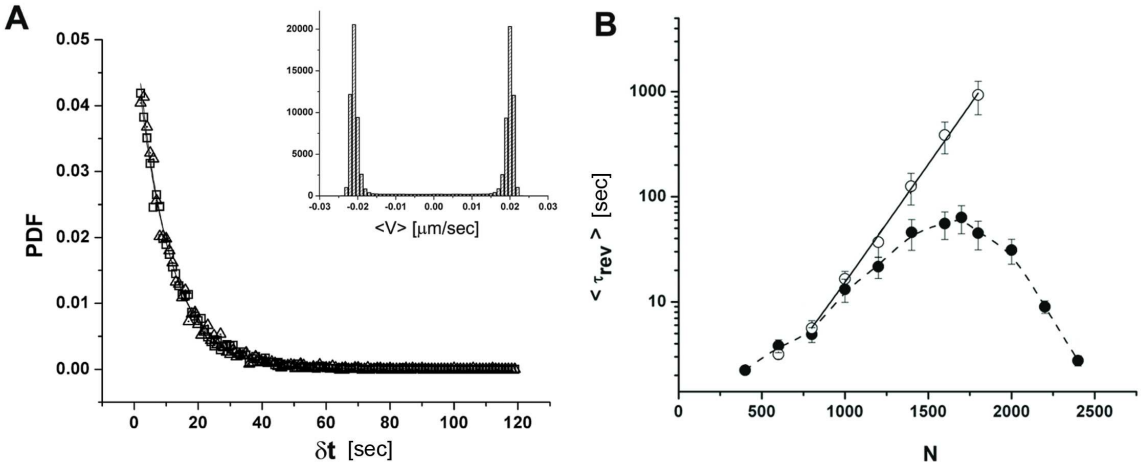

Figure 2.8: (A) The probability distribution function (PDF) of the reversal time corresponding to one track realization of $N = 1000$ motors. The distribution is fitted by a single exponential decay function (see Eq. 2.1). The insets show the velocity histogram which is symmetric with average velocities of $< v >= 0.02$ μm/sec and $< v >= -0.02$ μm/sec for bundles moving to the right and left respectively. (B) The mean reversal time $\langle \tau_{\rm rev} \rangle$ as a function of the number of motors N. For each value of N, the calculation of $\langle \tau_{\rm rev} \rangle$ is based on simulations of 40 different track realizations, where the error bars represent the standard deviation of $\tau_{\rm rev}$ between realizations. The solid and open circles denote the results corresponding to $\alpha = 0.002$ (our model) and $\alpha = 0$ (original model presented in ref. [1]), respectively. In the latter case $\langle \tau_{\rm rev} \rangle$ increases exponentially with N (as indicated by the solid straight line), while in the former case $\langle \tau_{\rm rev} \rangle$ exhibits a non-monotonic behavior (as indicated by the dashed line which serves as a guide to the eye) and reaches considerably lower values. Figure taken from Gur et al. [3].

Because the spacing between the motors is incommensurate with the periodicity of the potential, the total spatial distribution is uniform in x for $N \gg 1$:

$$p_{\rm att}(x,t) + p_{\rm det}(x,t) = \frac{1}{l}. \tag{2.11}$$

Using Eq. 2.11, together with Eqs. 2.9 and 2.10 to define the on and off rates in Eq. 2.8, the following steady-state equation ($\partial_t p = 0$) can be derived for $p_{\rm att}(x)$:

$$lv\frac{dp_{\rm att}(x)}{dx} = \begin{cases} -l\omega_1 p_{\rm att}(x) & \text{for } |x| \le a \\ \omega_2 - l\left(\omega_2 + \omega_3^0 \exp\left(\alpha N\right)\right) p_{\rm att}(x) & \text{for } a < |x| \le l/2. \end{cases} \tag{2.12}$$

Eq 2.12 should be solved subject to the boundary condition that $p_{\rm att}(-l/2) = p_{\rm att}(l/2)$ and the requirement that $p_{\rm att}(x)$ is continuous anywhere in the interval $-l/2 \le x \le l/2$, including at $x = \pm a$. Several solutions are plotted in Fig. 2.9 for $2a = 0.76l$ (see section 2.3), and three different sets of attachment and detachment rates: $\omega_3^0 = 0$, and $(\omega_1, \omega_2) = (v/l, v/l)$ (thin solid line), $(5v/l, 5v/l)$ (dashed line), and $(30v/l, 30v/l)$ (thick solid line). Those rates are taken to show the dependence of the probability density on the attachment and detachment rates, and do not, at this point, correspond to the rates presented in section 2.3.

The solutions in Fig. 2.9 correspond to the case when the motors move to the right ($v > 0$) and, therefore, it is easy to understand why $p_{\rm att}$ reaches its maximum at $x = -a$ (just before the motors enter, from the left, into the central gray-shaded detachment interval ($-a < x < a$)) and its minimum at $x = a$ (just before leaving the central detachment interval through the right side). We also notice that when the off rate $\omega_1 \gg v/l$, $p_{\rm att}$ drops very rapidly (exponentially) to near zero in the detachment interval. When the attachment rates $\omega_2 \gg v/l$, $p_{\rm att}$ increases exponentially fast for $x > a$ and rapidly reaches the maximum possible value $p_{\rm att} = 1/l$. The second steady state solution corresponding to the case when the motors move to the left ($v < 0$) is simply a mirror reflection of the first solution with respect to $x = 0$.

Each of the steady state solutions is characterized by $N_c = N \cdot P$ ($P \le 1$) connected

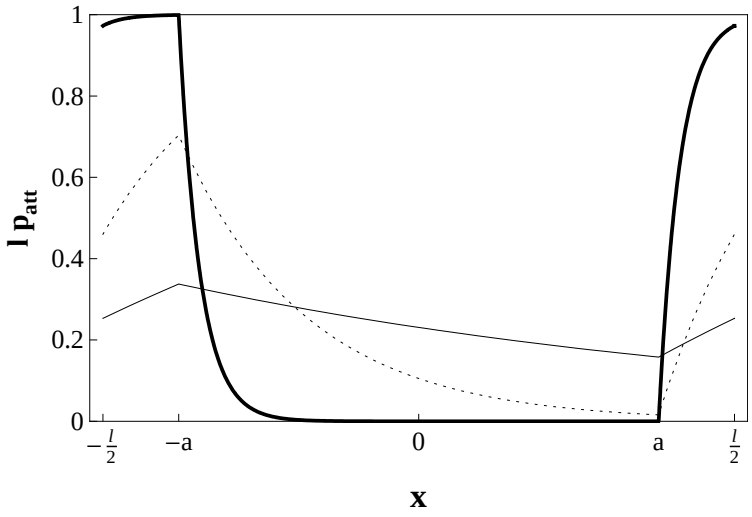

Figure 2.9: The steady state probability density, p_{att}, as a function of x, the position within a unit cell of the periodic potential. The functions plotted in the figure correspond to $2a = 0.76l$, $\omega_3^0 = 0$, and $(\omega_1, \omega_2) = (v/l, v/l)$ - thin solid line, $(\omega_1, \omega_2) = (5v/l, 5v/l)$ - dashed line, $(\omega_1, \omega_2) = (30v/l, 30v/l)$ - thick solid line. Figure taken from Gur et al. [3].

motors. Were N_c is the number of connected motors, and P, the mean probability to be in the connected state is obtained by integrating the function $p_{\rm att}(x)$ over the interval $-l/2 \leq x \leq l/2$

$$P = \int_{-l/2}^{l/2} p_{\rm att}(x)\, dx. \tag{2.13}$$

The population of connected motors can be divided into two groups: The connected motors which are located left to the minimum of the periodic potential ($-l/2 < x < 0$) experience forces pushing them to the right, i.e., forces directed in their direction of motion. Conversely, attached motors which are located right to the minimum experience forces directed opposite to their direction of motion. We will mark N_+ and $N_- = N_c - N_+ \leq N_+$ motors that, respectively, support and object the motion. Let us define the excess number of motors working in the direction of the motion as $N \cdot \Delta = N_+ - N_-$, where Δ will be termed the "bias parameter". The "bias parameter', can be related to $p_{\rm att}$ by

$$\Delta = \int_{-l/2}^{0} p_{\rm att}(x)\, dx - \int_{0}^{l/2} p_{\rm att}(x)\, dx. \tag{2.14}$$

Notice that P and Δ denote the averages of quantities (which we, respectively, denote by $P(t)$ and $\Delta(t)$) whose values fluctuate in time due to the stochastic binding and unbinding of motors. In order to derive an expression for the reversal time of the dynamics, we now consider the fluctuations of the instantaneous bias parameter, $\Delta(t)$, around the mean value Δ. The motors may switch their direction of motion when $\Delta(t) = 0$, i.e., when the motion momentarily stops. The occurrence probability of such an event can be related to the mean reversal by:

$$\tau_{\rm rev} \sim \left[\Pi\left(\Delta\left(t\right) = 0\right)\right]^{-1}. \tag{2.15}$$

To estimate $\Pi\left(\Delta\left(t\right) = 0\right)$ we proceed by noting that the probability of finding a motor attached left to the minimum of the potential, i.e. a motor experiencing a force directed in the direction of motion, is $P^+ = (P + \Delta)/2$. The probability that a motor is experiencing

a force directed opposite to the direction of motion is $P^- = (P - \Delta)/2$. The probability of having N_+ and $N_- \leq N_+$ motors which, respectively, support and object to the motion can thus be approximated by the trinomial distribution function

$$\pi(N_+, N_-) = \frac{N!}{N_+!N_-!(N - N_+ - N_-)!} \left(\frac{P + \Delta}{2}\right)^{N_+} \left(\frac{P - \Delta}{2}\right)^{N_-} (1-P)^{(N-N_+-N_-)}. \quad (2.16)$$

The instantaneous bias is given by $\Delta(t) = (N_+ - N_-)/N$, and the probability that $\Delta(t) = 0$ can be expressed as sum over the relevant terms in Eq. 2.16 for which $N_- = N_+$

$$\Pi(\Delta(t) = 0) = \sum_{i=0}^{N/2} \pi(i, i) = \sum_{i=0}^{N/2} \frac{N!}{(i!)^2(N - 2i)!} \left(\frac{P^2 - \Delta^2}{4}\right)^i (1 - P)^{(N-2i)}. \quad (2.17)$$

Replacing the sum in Eq. 2.17 by an integral, using Sterling's approximation for factorials, expanding the logarithm of the integrand in a Taylor series (up so second order) around the maximum which is at $i_{\max} = (N/2)\sqrt{P^2 - \Delta^2}/(1 - P + \sqrt{P^2 - \Delta^2})$ and then exponentiating the expansion, and finally extending the limits of integration to $\pm\infty$ (which has a negligible effect on the result for $N \gg 1$) - leads to:

$$\Pi(\Delta(t) = 0) = \left[1 - P + \sqrt{P^2 - \Delta^2}\right]^N \times \int_{-\infty}^{+\infty} dy \exp\left[-\frac{2}{C(1 - C)N} (y - i_{\max})^2\right], \quad (2.18)$$

where $C = \sqrt{P^2 - \Delta^2}/(1 - P + \sqrt{P^2 - \Delta^2})$. This yields

$$\tau_{\text{rev}} = \frac{2\tau_0}{\Pi(\Delta(t) = 0)} = 2\tau_0 \sqrt{\frac{2}{\pi C(1 - C)N}} \left[1 - P + \sqrt{P^2 - \Delta^2}\right]^{-N}, \quad (2.19)$$

where τ_0 is some microscopic time scale. The factor of 2 in the numerator in Eq. 2.19 is due to the fact that once the motors stop, they have equal probability to move in both directions. Eq. 2.19 predicts an almost exponential dependence of τ_{rev} on N only for constant values of P and Δ, which was the case in ref. [1]. In the more general case, the dependence of τ_{rev} on N can be derived by calculating the values of P and Δ as a function of N and substituting these values into Eq. 2.19.

To test the validity and accuracy of the analytical expression for τ_{rev}, we take the following steps: (i) set the model parameters l, a, ω_1, ω_2, ω_3^0, and α to the values used in the

computer simulations, section 2.3, (ii) calculate the probability density $p_{\rm att}$ corresponding to these values (Eq. 2.12) and use Eqs. 2.13 and 2.14 to calculate P and Δ over the range of N studied in the simulations, (iii) substitute the values of P and Δ into Eq. 2.19, to obtain $\tau_{\rm rev}$ as a function of N, (iv) fit the analytical expression for $\tau_{\rm rev}(N)$ to the simulation results plotted in Fig. 2.8B. This procedure involves two fitting parameters: the microscopic time scale τ_0 appearing in Eq. 2.19, and the group velocity v appearing in the steady-state equation (Eq. 2.12). A seemingly reasonable choice for the latter would be $v = 20$ nm/sec, which is where the velocity histogram of the bidirectional motion is peaked (see the insets of Fig. 2.8A). However, the motors slow down before each change in their direction of the motion; and because these changes in the directionality are fairly rare events, their occurrence probability is likely to be strongly influenced by the short periods of slow motion preceding them. Thus, it can be expected that the best fit of Eq. 2.19 to the simulation results is achieved for $v < 20$ nm/sec. Indeed, for $v = 8.2$ nm/sec and $\tau_0 = 680$ msec, we obtain the fitting curve shown in Fig. 2.10, which is an excellent agreement with our computational results for the reversal times (plotted in Fig. 2.8B and replotted here in Fig. 2.10) over the whole range of values of N investigated ($400 < N < 2400$). The steady state probability density, $p_{\rm att}(x)$, on the basis of which $\tau_{\rm rev}$ was calculated is shown in Fig. 2.11 for several different values of N ($N = 1000$ - solid line, $N = 2000$ - dashed line, $N = 2500$ - thick solid line). As can be seen from the figure, the detachment rate ω_1 in our simulations is so large that the central detachment interval of the unit cell ($-a < x < a$) is completely depleted of motors. Increasing N leads to a decrease in the effective attachment rate around the potential maximum, which reduces both the number of motors supporting ($-l/2 < x < -a$) and objecting ($a < x < l/2$) the motion and leads to the non-monotonic dependence of τ on N. The fitting value of $\tau_0 = 680$ msec is very close to $\tau^* = l/v = 5$ nm/(8 nm/sec) $= 625$ msec, which is the traveling time of the motors within a unit cell of the potential (once we set $v = 8.2$ nm/sec) and, therefore, is also the characteristic time scale at which the motors change their "states" (detached, connected and supporting the motion, connected

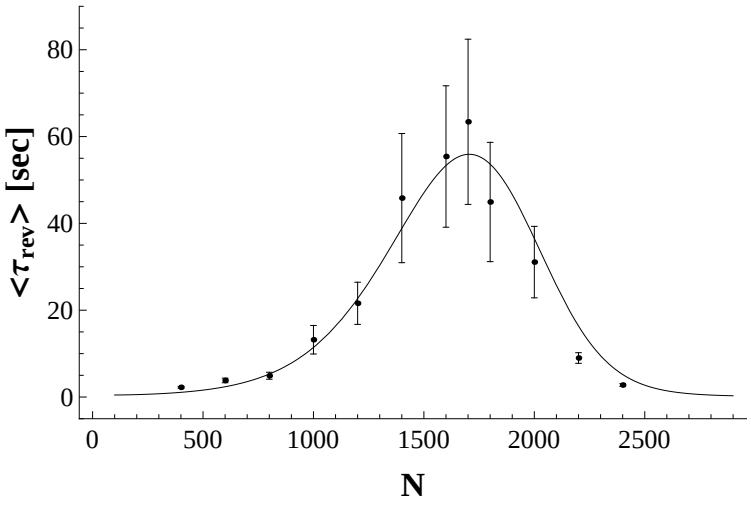

Figure 2.10: The reversal time $\langle \tau_{\rm rev} \rangle$ as a function of the number of motors N. The circles denote the simulations results (replotted from Fig. 2.8). The curve is a fit of the results to Eq. 2.19, with $\tau_0 = 680$ msec and $v = 8.2$ nm/sec. Figure taken from Gur et al. [3].

and objecting the motion). The remarkable agreement between the analytical and simulation results for $\tau_{\rm rev}$ should not, however, be allowed to obscure the fact that Eq. 2.19 is a master equation which, in principle, is not suitable for the calculating the probabilities of rare fluctuation events (such as velocity reversals in cooperative bidirectional movement). The agreement is achieved with effective velocity ($v = 8.2$ nm/sec) which is significantly smaller than the typical velocity measured in the simulations ($v = 20$ nm/sec). Therefore, one should not expect the steady state probability density $p_{\rm att}(x)$ plotted in Fig. 2.11 to perfectly match the simulations data.

For a slightly different set of model parameters, which are still valid for an actin II-myosin system [2], we could fit our analytical expression of the reversal time (Eq. 2.19), to the experimental results for a range of motors $400 < N < 3000$, see Fig. 2.13.

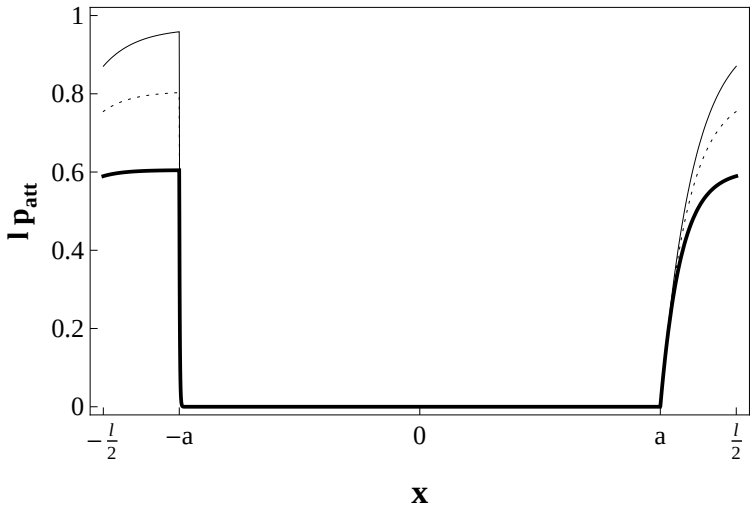

Figure 2.11: The steady state probability density $p_{\mathrm{att}}(x)$ computed for several values of N ($N = 1000$ - solid line, $N = 2000$ - dashed line, $N = 2500$ - thick solid line). The group velocity of the motors is $v = 8.2$ nm/sec, while the model parameters are set to the values used in the simulations (see section 2.2.2). Figure taken from Gur et al. [3].

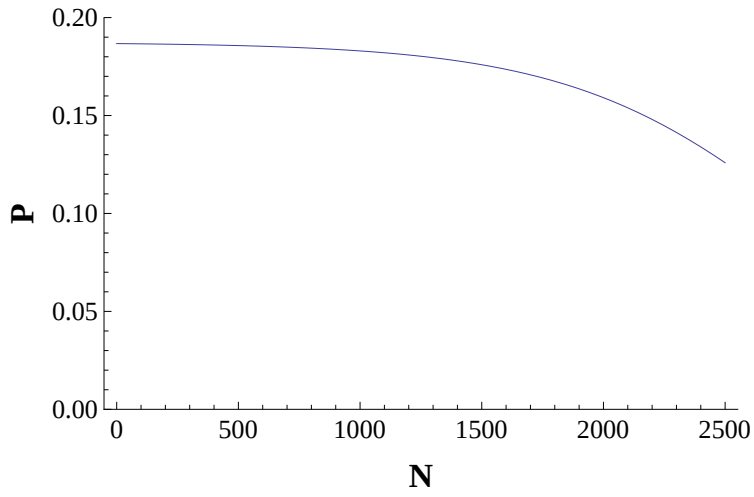

Figure 2.12: The probability of a motor to be in the connected state (defined in equation 2.13) as a function of N, the number of motors. The probability corresponds to our modified elastic model as explained in section 2.2.1. If the elasticity of the actin filament was not taken into account, the probability of a motor to be in the connected state would be constant with a value of P=0.187 (which is the value of P(N=0) in the plot).

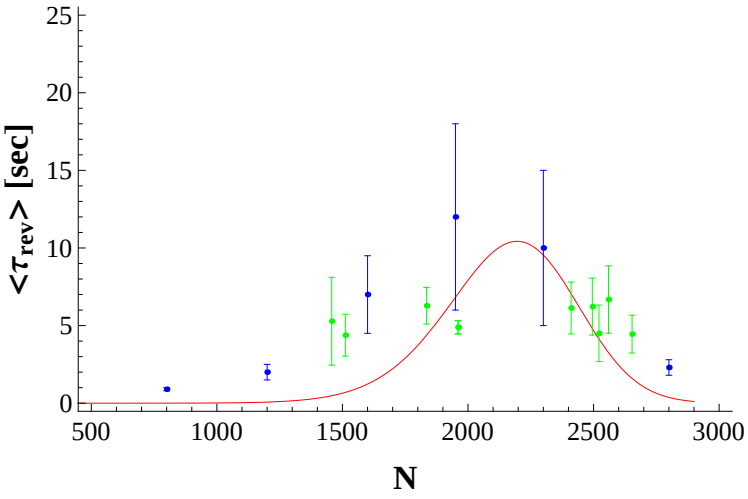

Figure 2.13: The reversal time $\langle \tau_{\text{rev}} \rangle$ as a function of the number of motors N. By taking a slightly different set of model parameters, which are still valid for an actin II-myosin system, we were able to reduce both the computed simulated results (in blue) and the analytical results (in red) to the range of the experimental results (in green). In this plot, we have fitted our analytical expression of the reversal time, τ_{rev}, (Eq. 2.19) to the experimental results.

2.5 Summary

We use a two-state ratchet model to study the cooperative bidirectional motion of myosin II motors on actin tracks with randomly alternating polarities. Our model is an extension of a model previously proposed by Badoual *et al.* to explain the macroscopically large reversal times measured in motility assays [1]. These time scales of velocity reversals are orders of magnitude longer than the microscopic typical stepping times of individual motors and can be understood as a result of collective effects in many-motor systems. The ratchet model that we use assumes that the motors are coupled mechanically but act independently, i.e., their binding to and unbinding from the cytoskeletal track are statistically uncorrelated. These assumptions lead to a predicted exponential increase of $\tau_{\rm rev}$ with N, the number of motors. Motivated by recent experiments which exhibit no such dependence of $\tau_{\rm rev}$ on N [2], we introduced a modified version of Badoual's model which accounts for an additional cooperative effect of the molecular motors and which eliminates the exponential increase of $\tau_{\rm rev}$ with N. This additional collective effect arises from the forces that the motors jointly exert on the actin and the associated mean elastic energy which scales as $E/K_BT \sim NN_C$ (where $N_C < N$ is the number of attached motors). This scaling relationship implies that the typical energy released when a motor is detaching from the track increases linearly with N and, therefore, the detachment rate in many-motor systems should be larger than the detachment rate of individual motors. We show, both computationally and analytically, that when this effect is taken into account and the detachment rate is properly redefined, the characteristic reversal time does not diverge for large N. Instead, $\tau_{\rm rev}$ exhibits a much weaker dependence on N and reaches a maximum at intermediate values of N.

While our model definitely improves the agreement with the experimental results (compared to the original model), further improvement is needed in order to eliminate the non-monotonic dependence of $\tau_{\rm rev}$ on N. One step in this direction may be to consider other forms of the off-rate ω_3 which are based on more accurate evaluations of the actin elastic

energy. In the present work, our analysis is based on the approximation that the detachment rate depends only on N (the total number of motors), but not on the instantaneous number of attached motors and their locations along the cytoskeletal track. As a final remark here we note that our analytical calculation probably leads to over-estimation of the effect of the "track-mediated" elastic interactions on the reversal times (which may explain the decrease in $\tau_{\rm rev}$ for large N). In a more detailed picture the motors which release higher energy will detach at higher rates, and the detachment of these "energetic" motors will lead to the release of much of the elastic energy stored in the actin track. By contrast, in our analytical treatment, the contribution of all the connected motors to the energy is the same. Therefore, within our analytical calculation, a larger number of motors must be disconnected at a higher frequency, which increases the "stochastic noise" in the system that reduced $\tau_{\rm rev}$.

Chapter 3

Biased bidirectional dynamics of a-polar filaments

In the previous chapter, when we performed the analytical calculation, we have ignored both: (i) the sequential order of the polarities of the monomers, and (ii) the positions along the filament where the pulling forces of motors are applied. Within that treatment, the bidirectional motion on perfectly a-polar tracks consisting of an equal number of monomers with right-pointing ("positive") and left-pointing ("negative") polarities has no bias, i.e., the intervals of motion in both directions occur with equal probability. In this chapter we discuss an interesting effect related to the elasticity of the actin. We show that a-polar elastic filaments may exhibit a biased bidirectional motion and achieve a net migration along the motors-coated surface. For myosin II-actin systems, we find that the drift velocity is typically 2-3 orders of magnitude smaller than the velocity of a single myosin II motor and is comparable with the speed by which the motors move the a-polar bundle cooperatively during the unidirectional intervals of motion. This newly identified mechanism of propagation may, therefore, be relevant to processes of active self-organization of cytoskeletal structures during which filaments are transported and joined with each other by MPs.

3.1 Active transport of a-polar elastic chains

To demonstrate the effect, we consider the chain illustrated in Fig. 3.1, consisting of N monomers connected by $(N-1)$ identical springs with a spring constant k. Each monomer may be either free and experience no pulling force ($f = 0$), or attached to one motor in which case it is subjected to a force of magnitude f which is directed to the right ($+f$) for monomers with positive polarities and left ($-f$) for monomers with negative polarities. The moving velocity of the filament is given by $V = f_{\text{total}}/\lambda$, where $f_{\text{total}} = \sum_{l=1}^{N} f_l$ is the sum of motor forces applied on the monomers and λ is the friction coefficient of the chain. A chain of N monomers has 2^N connection configurations, where each such configuration can be represented by a vector $\vec{C}$ of size N specifying the state (connected/disconnected) of each monomer. For example, a chain of 4 monomers in which the first and third monomers are connected to motors will be represented by $\vec{C} = (1, 0, 1, 0)$. Let us also introduce a vector $\vec{S}$ whose components are related to the polarities of the monomers. The vector $\vec{S} = (1, 1, -1, 1)$, for instance, corresponds to a chain of 4 monomers in which the polarities of the first, second, and fourth monomers is positive while the third monomer has a negative polarity. The drift velocity can be calculated by averaging over all possible connection configurations of the motors (all possible values of the vector $\vec{C}$):

$$V_{\text{drift}}(\vec{S}) \equiv \langle V \rangle = \sum_{j=1}^{2^N} \frac{f}{\lambda_j} \left(\vec{C}_j \cdot \vec{S} \right) P_j, \tag{3.1}$$

where P_j is the occurrence probability of the configuration, and the subscript j has been added to λ to account for possible variations in the friction coefficient between the different configurations. The probability P_j depends on (i) the number of attached motors in the configuration, $N_c(j) = \|\vec{C}_j\|^2$, (ii) the attachment probability of a single motor, ρ, and (iii) the total elastic energy of the springs E_j^{el}:

$$P_j = \frac{1}{Z} \rho^{N_c(j)} (1-\rho)^{(N-N_c(j))} e^{-\beta E_j^{\text{el}}}, \tag{3.2}$$

where $\beta = (k_B T)^{-1}$ is the inverse temperature and Z is the partition function of the system. The elastic energy is the sum of the energies of the springs, $E_j^{\rm el} = \sum_{i=1}^{N-1} F_i^2/2k$, where F_i is the force stretching (or compressing) the i-th spring. The forces F_i can be calculated using the following steps: (i) calculate the mean force $\bar{f} \equiv f_{\rm total}/N = f(\vec{C}\cdot\vec{S})/N$, (ii) calculate the access forces acting on the monomers $f_l^* = fC_lS_l - \bar{f}$, and (iii) sum the access forces applied on all the monomers located on one side of the spring $F_i = \sum_{l=1}^{i} f_l^* = -\sum_{l=i+1}^{N} f_l^*$. Our analysis is based on the assumption that variations in $\vec{C}$ (which occur when motors attach to or detach from the actin track) lead to instantaneous changes in the velocity of the filament which should always be proportional to the total exerted force. This assumption is expected to hold for low Reynolds numbers where inertia can be neglected.

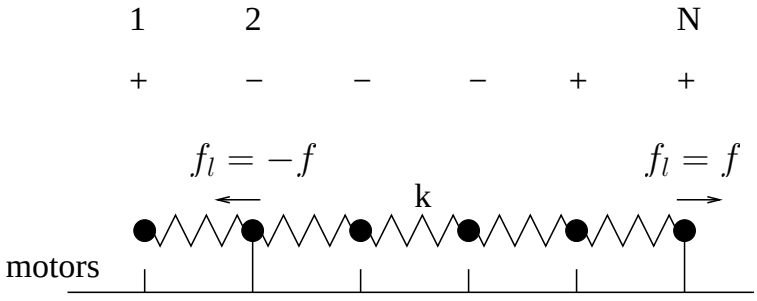

Figure 3.1: A schematic drawing of the system: A chain of consisting of N monomer connected to each other by $N-1$ identical springs. The chain lies on a "bed" of motors, some of which are connected to the monomers. A connected monomer with positive (negative) polarity feels a pulling force of size $+f$ $(-f)$. Disconnected monomers experience no force. Figure taken from Gur and Farago [4].

3.2 Analysis of the $N = 4$ case

For a better understanding, it will be useful to examine a short chain of size $N = 4$. There are six different a-polar sequences for a chain of this length: $\vec{S}_{1a} = -\vec{S}_{1b} = (1, 1, -1, -1)$,

$\vec{S}_{2a} = -\vec{S}_{2b} = (1,-1,1,-1)$, $\vec{S}_{3a} = -\vec{S}_{3b} = (1,-1,-1,1)$. It is easy to prove that the drift velocity (see Eqs. (3.1) and (3.2)) vanishes for the first four sequences which are antisymmetric with respect to reflection around the midpoint. This is not the case with the last two symmetric configurations. To see this, consider the sequence $\vec{S}_{3a}$ and assume, for simplicity, that $\lambda_j = \lambda$. In the limit $\rho \ll 1$, one can ignore the configurations in which more than one monomer is connected to a motor. There are, therefore, only five possible configurations:
(i) $\vec{C}_j = (0,0,0,0)$, for which $V_j = 0$ and $P_j = (1-\rho)^4/Z$.
(ii) $\vec{C}_j = (1,0,0,0)$ and $\vec{C}_j = (0,0,0,1)$, for which $V_j = f/\lambda$ and $P_j = \rho(1-\rho)^3 e^{-(7/8)(\beta f^2/2k)}/Z$.
(iii) $\vec{C}_j = (0,1,0,0)$ and $\vec{C}_j = (0,0,1,0)$, for which $V_j = -f/\lambda$ and $P_j = \rho(1-\rho)^3 e^{-(3/8)(\beta f^2/2k)}/Z$.
Substituting this in Eq. (3.1) gives $V_{\rm drift}(\vec{S}_{3a}) = -V_{\rm drift}(\vec{S}_{3b}) \simeq -2(f/\lambda)\rho[e^{-(3/8)(\beta f^2/2k)} - e^{-(7/8)(\beta f^2/2k)}]$. For $\beta f^2/2k \ll 1$ we find that the drift velocity increases with a third power of the motor force, $V_{\rm drift} \simeq (\beta/2k\lambda)f^3$. This power law has a different exponent than 1 – the scaling exponent for the velocity of stiff polar chains.

3.3 Long chains

To further investigate this effect, we calculated the drift velocity for chains of $N = 4M$ monomers with sequences of the form $\vec{S} = (\overbrace{-1,\ldots,-1}^{M},\overbrace{1,\ldots,1}^{2M},\overbrace{-1,\ldots,-1}^{M})$. Our results are summarized in Figs. 3.2(A) and (B). Fig. 3.2(A) is based on a calculation in which the friction coefficient (see Eq. (3.1)), $\lambda_j = \lambda_0 N$, while in Fig. 3.2(B), we assumed that $\lambda_j = \lambda_0 N_c(j)$. The results for $N \leq 28$ have been derived using a full statistical calculation of the partition function, while for larger N they have been obtained from Metropolis Monte Carlo simulations. The model parameters were assigned the following values which are representative of myosin II-actin systems [3, 83]: $\beta f^2/2k = 0.002$, $\rho = 0.1$, and the speed of a single motor, $v = f/\lambda_0 = 6$ μm/sec. Both figures show that for small chains of size $N < 200$, the drift velocity increases rapidly with N. For larger chains ($N > 200$), $V_{\rm drift}$

behaves differently in Figs. 3.2(A) and (B). In the former it decreases with N, while in the latter it saturates and increases again for $N > 600$. Note also the different scales of the y-axis in both figures. These differences can be attributed to the different values of λ_j used in the cases represented by Figs. 3.2(A) and (B). Since for each configuration, the ratio between the friction coefficients in both cases $r_\lambda \equiv \lambda_j^B/\lambda_j^A = N_c(j)/N \leq 1$, the drift velocity in (B) must always be larger than in (A). Fig. 3.3 depicts the mean value of r_λ (i.e., the mean fraction of connected monomers) as a function of N. For $N < 50$, $\langle r_\lambda \rangle \simeq \rho = 0.1$ and, accordingly, the ratio between the drift velocities in (B) and (A) in this region is close to one order of magnitude. For $N > 50$, $\langle r_\lambda \rangle$ drops to values much smaller than ρ, which implies that the friction coefficient *per monomer* decreases with N in case (B) and explains why the drift velocity remains high and does not decrease sharply as in (A). The decrease in the mean fraction of connected monomers can be traced to the fact that configurations with larger $N_c(j)$ have, in general, higher elastic energies and, therefore, smaller statistical weights. For the mean elastic energy, $E_j^{\rm el}/k_BT = c(\beta f^2/2k)NN_c(j)$ [2, 3], one gets

$$\langle r_\lambda \rangle = \left\langle \frac{N_c}{N} \right\rangle = \frac{\rho \exp(-cN\beta f^2/2k)}{1 - \rho[1 - \exp(-cN\beta f^2/2k)]}, \tag{3.3}$$

where c is a dimensionless constant of the order of 1. For $c = 0.75$ and $N \leq 1000$, this expression (solid line in Fig. 3.3) gives a fair agreement with the computational results. For larger values of N (i.e., when $\langle N_c/N \rangle$ becomes very small), the expression tends to overestimate the rate of decrease in the mean fraction of connected monomers (or, equivalently, the effective attachment probability). The decrease in the attachment probability of the motors is another, indirect, manifestation of cooperativity between the motors which is mediated through the forces that they jointly exert on the actin track. Eq. (3.3) suggests that the elasticity of the track can be neglected for small filaments whose size $N \ll (\beta f^2/2k)^{-1} \equiv N^*$. In this regime, the two cooperativity effects discussed here which are associated with the elasticity of the actin filaments disappear: (i) The drift velocity $V_{\rm drift} \sim (\beta/2k\lambda)f^3 = (f/\lambda)(N^*/N) \ll (f/\lambda)$ is vanishingly smaller than the typical speed by which the bidirectionally moving bundle

propagates in each direction, and (ii) the fraction of attached motors $\langle N_c/N \rangle \simeq \rho$ is very close to the attachment probability of individual motors. The elasticity effects can be detected only for long filaments with $N \gtrsim N^*$, which are softer (the effective force constant of the filament decrease as N^{-1}) and, hence, more influenced by the forces of the motors. For infinitely stiff filaments ($k \to \infty$), the crossover filament size diverges ($N^* \to \infty$) and the filament elasticity is, of course, irrelevant on all length scales.

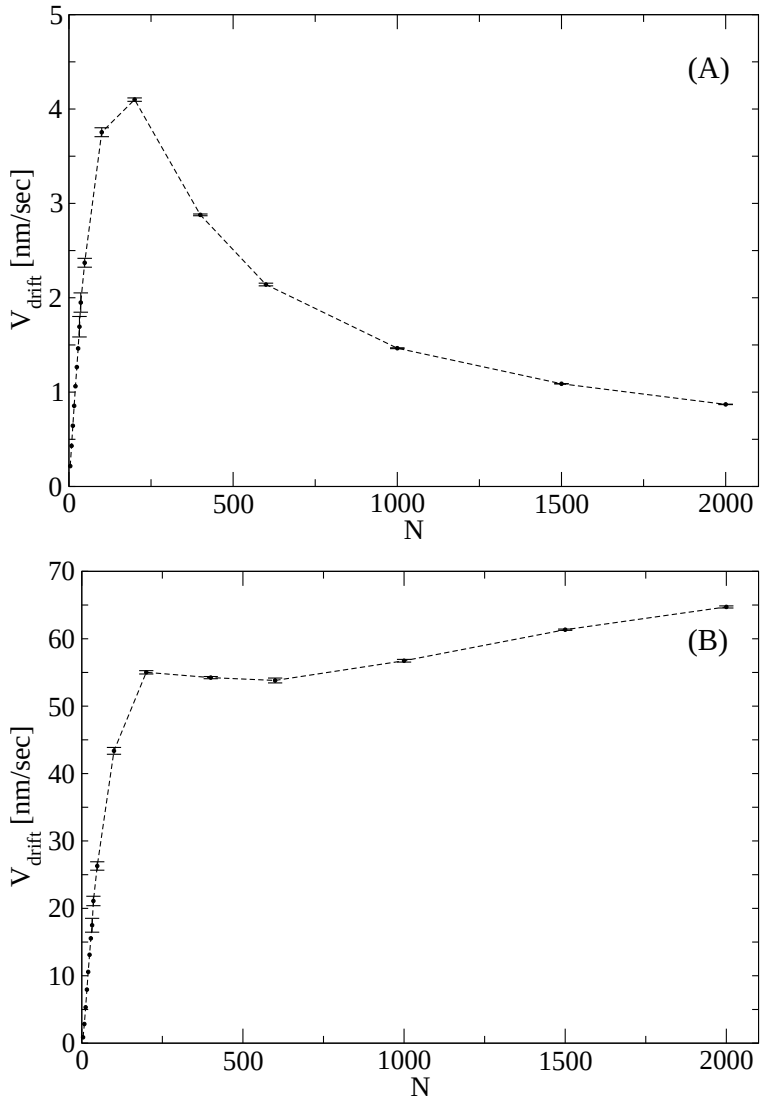

Figure 3.2: The drift velocity V_{drift} as a function of the length of the chain. The friction coefficient λ_j is proportional to the number of monomers N in (A) and the number of connected motors $N_c(j)$ in (B). The lines are guides to the eye. Figure taken from Gur and Farago [4].

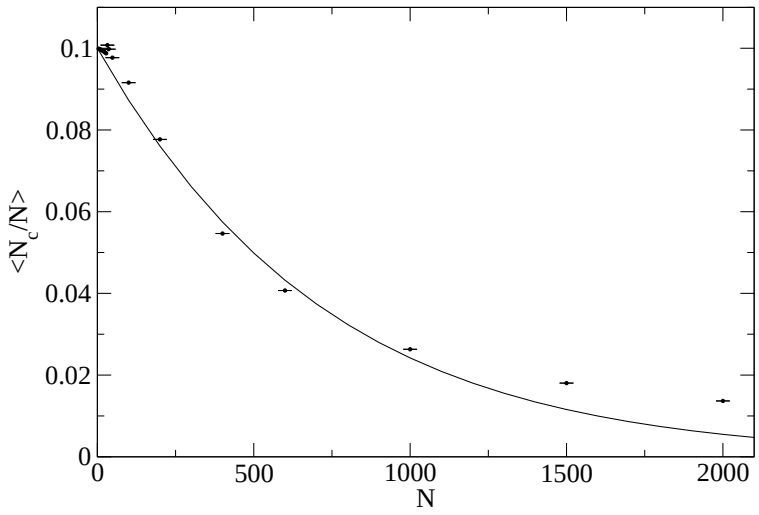

Figure 3.3: The mean fraction of monomers connected motors, $\langle N_c/N \rangle$ as a function of N. The solid line represents Eq.(3.3) with $c = 0.75$. Figure taken from Gur and Farago [4].

3.4 Summary

Figs. 3.2(A) and (B) represent two limiting cases. In the former, the friction is caused by the drag of the actin bundle in the viscous environment, while in the latter it originates from the attachment of the actin to the underlying surface of motors. The actual friction coefficient is expected to lie between these two extreme values and, therefore, the drift velocity should exhibit an intermediate behavior between those shown in Figs. 3.2(A) and (B). Thus, the typical magnitude of V_{drift} is expected to be of the order of 10 nm/sec. Interestingly, the drift velocity of the bundle is of the same order of magnitude as its speed during the bidirectional motion [2], which has also been found to be 2-3 order of magnitude smaller than the moving velocity of individual myosin II motors ($v \sim 6$ μm/sec [83]). Over a period of a few minutes the a-polar bundle may progress a distance of a few micrometers. This implies that the drift of a-polar bundles may be relevant to the active remodeling of the cell cytoskeleton occurring

during many cellular processes.

Our investigation of the role of the filament elasticity in modifying collective motion of molecular motors has been motivated by experiments which have been described and analyzed in chapter 2. In this chapter we presented a more realistic microscopic based model that involves the determination of the exact elastic energy of the filaments. We demonstrated that such a model leads to new insights and novel results like the biased transport of filaments with no net polarities. Experimental verification of this surprising result is, however, difficult. It requires that (i) the moving filaments are perfectly a-polar with internal (sequential) order, and (ii) that they move for sufficiently long period of time such that the net drift can be extracted from the statistics of the unidirectional intervals of motion. Unfortunately, the a-polar bundles are not formed by a well controlled process, but rather through a sequence of stochastic fusion events that usually generate filaments with disordered, random, sequences and with little residual polarities [2]. Also, in the existing experimental setup, the bidirectional motion cannot be tracked for more than about 10 minutes, which is too short for a meaningful statistical analysis. What should be more experimentally testable is the other elasticity effect, namely the reduction in the fraction of connected motors. This effect, which has been attributed to the dependence of the elastic energy on the configuration of connected motors (denoted by the vector $\vec{C}$), is not limited to a-polar filaments. Polar filaments experiencing a non-uniform distribution of motor forces (i.e., when only a fraction of the monomers are connected to motors) will also develop a tensile stress that could potentially alter the attachment probability of the motors. In a future publication we plan to present a theoretical analysis of the attachment probability for perfectly polar filaments, similar to the analysis presented here for a-polar filaments. We also plan to investigate this effect experimentally by using a motility assay combined with micro-manipulation technique (such as optical tweezers) to stall the gliding filament and measure the mean force generated by the motors. In the case of perfectly polar filaments,

the forces of all the motors are applied along the same direction and, therefore, the total measured force should be simply proportional to the number of attached motors.

Chapter 4

Discussion

In recent years, there has been a growing focus on the cooperative action of protein motors. This type of research is motivated by the fact that the mechanism behind such systems is not yet fully understood, and that its understanding is relevant for many biological systems such as cell motility, muscle contraction, mitosis, the movement of the flagellum etc. In this thesis, we have focused on cooperative effects which are associated with the elastic properties of the actin filaments. We have shown that the elastic energy of the system scales linearly with N, the number of motors, Eq. 2.5. therefore, longer filaments will have a higher elastic energy which will lead to a smaller fraction of connected motors as we have shown in Fig. 3.3. In chapter 2 we have studied how this effect influences the bidirectional dynamics of a-polar filaments. This elastic effect caused τ_{rev} to have a weakly depends on the length of the chain. Our result, which is with contradiction to a previous theoretical result (that don't take into account the elasticity of the actin filaments) [1], is supported by recent experimental evidence [2]. In chapter 3 we have performed a more detailed calculation which takes into account both the sequential order of the polarities and the positions along the filament where the pulling forces of the motors were applied. Surprisingly, we have found that the dynamics of the filaments is not only depended on the total polarity, but depends on

the internal sequence of the polar monomers that assemble the filament, and that perfectly a-polar filaments show a bidirectional dynamics with a non vanishing drift velocity.

The *elastic ratchet* model which we have presented in this work can, perhaps, be further extended in order to describe other related problems such as:
(i) The intermediate fusing process: In the experiment, the polar bundles are formed by a sequence of events. Originally, we have polar segments that move unidirectionally and fuse with each other. At later stages, the system consists of a-polar bundles who move bidirectional. However, from time to time, a filament that moves bidirectional, may suddenly exhibit a fast unidirectional motion which would end up in a fusion with a distant filament. This sudden transition from bidirectional to directional motion, is clearly driven by some filament-filament interaction. If we will be able to identify the source and form of this interaction, we could introduce it into our model to theoretically rebuild this sudden transition.
(ii) Directional transport on elastic polar filaments: In this thesis we have focused on the bidirectional motion of a-polar filaments, which is a natural playground when studying cooperative dynamic effects. However, the concept of elasticity, as it has been presented in this work, should also affect the unidirectional dynamics of polar filaments and therefore, we believe that expanding the model in this direction is only natural.
(iii) Systems with high protein friction: Our analysis in chapter 2 which coarse grains many molecular features into a small number of model parameters, can be rebuilt in a more detailed way, were λ, the friction coefficient, will not be constant but would depend on the length of the filament and the state of the motors, by doing so, the model could be used to describe systems with dynamics that is strongly governed by protein friction.

Bibliography

[1] M. Badoual, F. Jülicher and J. Prost, *Proceedings of the National Academy of Sciences* **99**, 6696 (2002).

[2] B. Gilboa, D. Gillo, O. Farago and A. Bernheim-Groswasser, *Soft Matter* **5**, 2223 (2009).

[3] B. Gur, D. Gillo, A. Bernheim-Groswasser and O. Farago, *Physical Review E* **80**, 021929 (2009).

[4] B. Gur and O. Farago, *Physical Review Letters* **104**, 238101 (2010).

[5] P.B. Moore, H.E. Huxley and D.J. DeRosier, *Journal of Molecular Biology* **50**, 279 (1970).

[6] E. Frixione, *Cell Motility and the Cytoskeleton* **46(2)** 73 (2000)

[7] Y.L. Shin and L. Rothfield, *Microbiology and Molecular Biology Review* **70(3)**, 729 (2006).

[8] L. A. Amos and A. Klug, *Journal of Cell Science* **14**, 523 (i974).

[9] H.P. Erickson, *Journal of Cell Biology* **60**, 153 (1974).

[10] S. Heins, P.C. Wong, S. Muller, K. Goldie, D.W. Cleveland and U. Aebi, *Journal of Cell Biology* **123**, 1517 (1993).

[11] D.A.D Parry and P.M Steinert. *Intermediate filament structure* Springer-Verlag, New York. (1995).

[12] N. Geisler , J. Schünemann , K. Weber , M. Häner and U. Aebi, *Journal of Cell Biology* **282(3)**, 601 (1998).

[13] B. Alberts, D. Bray, J. Lewis, M. Raff, K. Roberts, and J.D. Watson, *Molecular Biology of the Cell* Garland, New York (1994).

[14] R.W. Lymn and E.W. Taylor,*Biochemistry* **10(25)**, 4617 (1971).

[15] I. Rayment, H.M. Holden, M. Whittaker, C.B. Yohn, M. Lorenz, K.C. Holmes and R.A. Milligan, *Science* **261**, 58 (1993).

[16] A.F. Huxley, *Prog Biophys Biophys Chem* **7**, 255 (1957).

[17] M. Büttiker, *Zeitschrift für Physik B: Condensed Matter* **68** 161 (1987).

[18] R. Landauer, *Journal of Statistical Physics* **53**, 233(1988).

[19] M.O. Magnasco, *Physical Review Letters* **71**, 1477 (1993).

[20] C.R. Doering, W. Horsthemke and J. Riordan, *Physical Review Letters* **72**, 2984 (1994).

[21] M.O. Magnasco, *Physical Review Letters* **72**, 2656(1994).

[22] M.M. Millonas and D.I. Dykman, *Physical Review Letters A* **183**, 65(1994).

[23] D.R. Chialvo and M.M. Millonas, *Physical Review Letters A* **209**, 26(1995).

[24] J. Luczka, R. Bartussek, and P. Hänggi, *Europhysics Letters* **31**, 431 (1995).

[25] A. Mielke, *Annals of Physics (Leipzig)* **4**, 476(1995a).

[26] A. Mielke, *Annals of Physics (Leipzig)* **4**, 721(1995b).

[27] M.M. Millonas, *Physical Review Letters* **74**, 10 (1995).

[28] R. Bartussek, P. Reimann, and Hänggi, *Physical Review Letters* **76**, 1166(1996).

[29] A. Ajdari, Ph.D. thesis (Université de Paris 6) (1992).

[30] A. Ajdari and J. Prost, *C. R. Acad. Sci. Paris II* **315**, 1635 (1992).

[31] R.D. Astumian and M. Bier, *Physical Review Letters* **72**, 1766 (1994).

[32] C.R. Doering, *Nuovo Cimento* **17**, 685(1995).

[33] J.F. Chauwin, A. Ajdari, and J. Prost, *Europhysics Letters* **27**, 421 (1994).

[34] C.S. Peskin, G.B. Ermentrout, and G.F. Oster, *Cell Mechanics and Cellular Engineering* Springer, New York p. xxx (1994).

[35] J. Prost, J.F. Chauwin, L. Peliti, and A. Ajdari, *Physical Review Letters* **72**, 2652(1994).

[36] H.X. Zhou and Y. Chen, *Physical Review Letters* **77**, 194 (1996).

[37] T. Harms and R. Lipowsky, unpublished (1997).

[38] T. Kreis and R. Vale, *Guidebook to the Cytoskeletal and Motor Proteins* (Oxford Univ. Press, New York) (1999).

[39] M.A. Geeves and K.C. Holmes, *Annual Review of Biochemistry* **68**, 687 (1999).

[40] M.P. Sheetz and J.A. Spudich, *Nature* **303** 31 (1983).

[41] J.A. Spudich, S.J. Kron and M.P. Shetz, *Nature* **315**, 584 (1985).

[42] M.V. Smoluchowski, Experimentell nachweisbare, der Ublichen Thermodynamik widersprechende Molekularphenomene, Physik. Zeitschr. 13 (1912) 1069.

[43] R.P. Feynman, R.B. Leighton and M. Sands, *The Feynman Lectures on Physics*, **1**, (Chapter 44, 46) (1963).

[44] T. Funatsu, Y. Harada, M. Tokunaga, K Salto and T. Yanagida, *Nature* **374(6522)**, 555 (1995).

[45] R.D Vale, *Journal of Cell Biology* **135**, 291 (1996).

[46] D.W Pierce, N. Hom-Booher and R.D Vale, *Nature* **388**, 338 (1997).

[47] T.R. Kelly, I. Tellitu and J.P. Sestelo, *Angewandte Chemie International Edition in English* **36(17)**, 1866 (1997).

[48] T.R. Kelly, J.P. Sestelo and I. Tellitu, *Journal of Organic Chemistry* **63**, 3655 (1998).

[49] K.L. Sebastian, *Physical Review E* **61** 937 (2000).

[50] O. Campás, Y. Kafri, K.B. Zeldovich, J. Casademunt and J.F. Joanny, *Physical Review Letters* **97**, 38101 (2006).

[51] F. Jülicher and J. Prost, *Physical Review Letters* **73**, 2618 (1995).

[52] F. Jülicher and J. Prost, *Physical Review Letters* **78**, 4510 (1997).

[53] R.M. da Silva, C.C. de Souza Silva and S. Coutinho, *Physical Review E* **78**, 61131 (2008).

[54] F. Jülicher, A. Ajdari and J. Prost, *Reviews of Modern Physics* **69**, 1269 (1997).

[55] F. Slanina, *Europhysics Letters* **84**, 50009 (2008).

[56] S.A. Endow and H. Higuchi, *Nature* **406**, 913 (2000).

[57] L. Tao, A. Mogliner, G. Civelekoglu-Scholey, R. Wollman, J. Evans, H. Stahlberg and J.M. Scholey, *Current Biology* **16**, 2293 (2006).

[58] D. Riveline, A. Ott, F. Jüicher, D.A. Winklemann, O. Cardoso, J.J. Lacapüe, S. Magnúsdóttir, J.L. Viovy, L. Gorre-Talini and J. Prost, *European Biophysics Journal* **27**, 403 (1998).

[59] S.P. Gross, M. Carolina Tuma, S.W. Deacon, A.S. Serpinskaya, A.R. Reilein and V.L. Gelfand, *Journal of Cell Biology* **156**, 855 (2002).

[60] D. Chowdhury, *Physica Scripta* **T106**, 13 (2003).

[61] A. Parmeggiani, T. Franosch and E. Frey, **Physical Review Letters 90**, 86601 (2003).

[62] S. Muhuri and I. Pagonabarraga, *Europhysics Letters* **84**, 58009 (2008).

[63] D. Chowdhury, A. Garai and J. S. Wang, *Physical Review E* **77**, 50902(R) (2008).

[64] D.G. Lichtenthaler and C. Goldman, *Condensed Matter* **803**, 2732 (2008).

[65] M. Ebbinghaus and L. Santen, *Condensed Matter* **901**, 183 (2009).

[66] S. Klumpp and R. Lipowsky, *Proceedings of the National Academy of Sciences* **102**, 17284 (2005).

[67] M.J.I. Müller, S. Klumpp and R. Lipowsky, *Proceedings of the National Academy of Sciences* **105**, 4609 (2008).

[68] Y. Zhang, *Condensed Matter* **901**, 350 (2009).

[69] D. Hexner and Y. Kafri, *Condensed Matter* **903**, 312 (2009).

[70] S.J. Kron and J.A. Spudich, *Proceedings of the National Academy of Sciences* **83**, 6272(1986).

[71] D.A. Smith and M.A. Geeves, *Biophysical Journal* **69**, 524 (1995).

[72] T.A.J. Duke, *Proceedings of the National Academy of Sciences* **96**, 2770 (1999).

[73] G. Lan and S.X. Sun, *Biophysical Journal* **88**, 4107 (2005).

[74] R.E.L. De Ville and E. Venden-Eijnden, *Bulletin of Mathematical Biology* **70**, 484 (2008).

[75] P.G. de Gennes, *Scaling Concepts in Polymer Physics* (Cornell Uni. Press, Ithaca) (1997).

[76] J.T. Finer, R.M. Simmons and J. A. Spudich, *Nature* **368**, 113 (1994).

[77] J.E. Molloy, J.E. Burns, J. Kendrick-Jones, R.T. Tregear and D.C. White, *Nature* **378**, 209 (1995).

[78] A.D. Mehta, J.T. Finer, and J.A. Spudich, *Proceedings of the National Academy of Sciences* **94**, 7927 (1997).

[79] C.M. Veigel, M.L. Bartoo, D.C. White, J.C. Sparrow and J.E. Molloy, *Biophysical Journal* **75**, 1424 (1998).

[80] M.J. Tyska, D.E. Dupuis, W.H. Guilford, J.B. Patlak, G.S. Waller, K.M. Trybus, D.M. Warshaw, and S. Lowey, *Proceedings of the National Academy of Sciences* **96**, 4402 (1999).

[81] J A. Millar and M.A. Geeves, *Nature* **312**, 232 (1983).

[82] J.W. Cardon and P.D. Boyer, *European Journal of Biochemistry* **92**, 443 (1978).

[83] J. Howard, *Mechanics of Motor Proteins and the Cytoskeleton* (Sinauer Press, Sunderland, Mass) (2001).